

# Radiogenomics for Precision Medicine With a Big Data Analytics Perspective

Andreas S. Panayides Senior Member, IEEE, Marios S. Pattichis, Senior Member, IEEE, Stephanos Leandrou Costas Pitris Member, IEEE, Anastasia Constantinidou, and Constantinos S. Pattichis Fellow, IEEE

**Abstract**—Precision medicine promises better healthcare delivery by improving clinical practice. Using evidence-based substratification of patients, the objective is to achieve better prognosis, diagnosis, and treatment that will transform existing clinical pathways toward optimizing care for the specific needs of each patient. The wealth of today's healthcare data, often characterized as big data, provides invaluable resources toward new knowledge discovery that has the potential to advance precision medicine. The latter requires interdisciplinary efforts that will capitalize the information, know-how, and medical data of newly formed groups fusing different backgrounds and expertise. The objective of this paper is to provide insights with respect to the state-of-the-art research in precision medicine. More specifically, our goal is to highlight the fundamental challenges in emerging fields of radiomics and radiogenomics by reviewing the case studies of Cancer and Alzheimer's disease, describe the computational challenges from a big data analytics perspective, and discuss standardization and open data initiatives that will facilitate the adoption of precision medicine methods and practices.

**Index Terms**—Precision medicine, quantitative imaging, radiomics, radiogenomics, cancer, Alzheimer, big data, deep learning.

## I. INTRODUCTION

PRECISION medicine aspires to leverage new knowledge emanating from heterogeneous imaging, genomic, environmental, and clinical data analysis, facilitating increased

Manuscript received February 15, 2018; revised June 13, 2018 and September 17, 2018; accepted October 15, 2018. Date of publication December 25, 2018; date of current version September 4, 2019. This work was supported by the Integrated Precision Medicine Technologies (IPMT) project, H2020-WIDESPREAD-04-2017-Teaming Phase 1, under Grant 763781. (*Corresponding author: Andreas S. Panayides.*)

A. S. Panayides and C. S. Pattichis are with the Department of Computer Science, University of Cyprus, Nicosia 2109, Cyprus (e-mail: panayides@cs.ucy.ac.cy; pattichi@ucy.ac.cy).

M. S. Pattichis is with the Department of Electrical and Computer Engineering, University of New Mexico, Albuquerque, NM 87131 USA (e-mail: pattichi@unm.edu).

S. Leandrou is with the Department of Health Sciences, European University Cyprus, Nicosia 2404, Cyprus, and also with School of Mathematical Sciences, Computer Science and Engineering, City, University of London, London WC1E 7HU, U.K. (e-mail: s.leandrou@euc.ac.cy).

C. Pitris is with the Department of Electrical and Computer Engineering, University of Cyprus, Nicosia 2109, Cyprus (e-mail: cpitris@ucy.ac.cy).

A. Constantinidou is with the Medical School, University of Cyprus, Nicosia 2109, Cyprus and also with the , BOC Oncology Centre, Nicosia 2006, Cyprus (e-mail: constantinidou.anastasia@ucy.ac.cy).

Digital Object Identifier 10.1109/JBHI.2018.2879381

understanding of disease progression, treatment efficacy, and prevention, towards developing new, personalized therapies and interventions (see Fig. 1). Such a radical shift in clinical care practice requires fundamental advances across a number of inter- and multi- disciplinary and cross-sectoral fields. Such advances range from the development of new big data analytics tools and research in precision medicine, to standardization of acquisition, storage, and open sharing of de-identified patients' electronic health records (EHR) and research data, as well as significant patient involvement (self-assessment and reporting) and supportive policies. Based on the above, precision medicine initiatives across both the EU and the USA have been formed with the end goal of promoting advances and developing a global understanding of precision medicine [1]–[3]. They emphasize on the potential quality of life (QoL) benefits for both patients and informal care givers, as well as the broader socioeconomic impact. Precision medicine has the potential to significantly reduce healthcare expenditures, while claiming a steadily increasing global market share, projected to reach \$141.7 billion by 2026, with a compound annual growth rate (CAGR) of 11.23% [4].

From a technical perspective, the challenge stems for heterogeneous data integration and joint processing to support new knowledge discovery. Key to precision medicine advances, genomic analysis and molecular profiling, is a computationally intensive task. Similarly, radiomics generate a plethora of quantitative image features presenting a different set of challenges [5]–[9]. At the same time, there is a strong need to consider computationally efficient methods to support joint mining of radiomics, genomics, and clinical data (see Fig. 1), and to support the discovery of synergistic patterns between radiomics and genomics, also termed radiogenomics [10]–[13].

Radiogenomics experienced tremendous growth over the past decade and demonstrated significant potential for developing non-invasive prognostic and diagnostic methods, identifying biomarkers for treatment, especially for cancer, by associating quantitative imaging features for tumor phenotyping and genomic signatures. Additionally, imaging methods were integrated with systems biology [14], [15].

Big data programming models and deep learning [16] paradigms are instrumental to radiogenomics research, not only to leverage computationally intensive tasks, but most importantly to contribute to new algorithms, methods, and workflows development, via efficient data acquisition, storage, sharing, and indexing [17]–[26]. Taking advantage of large datasets, deep

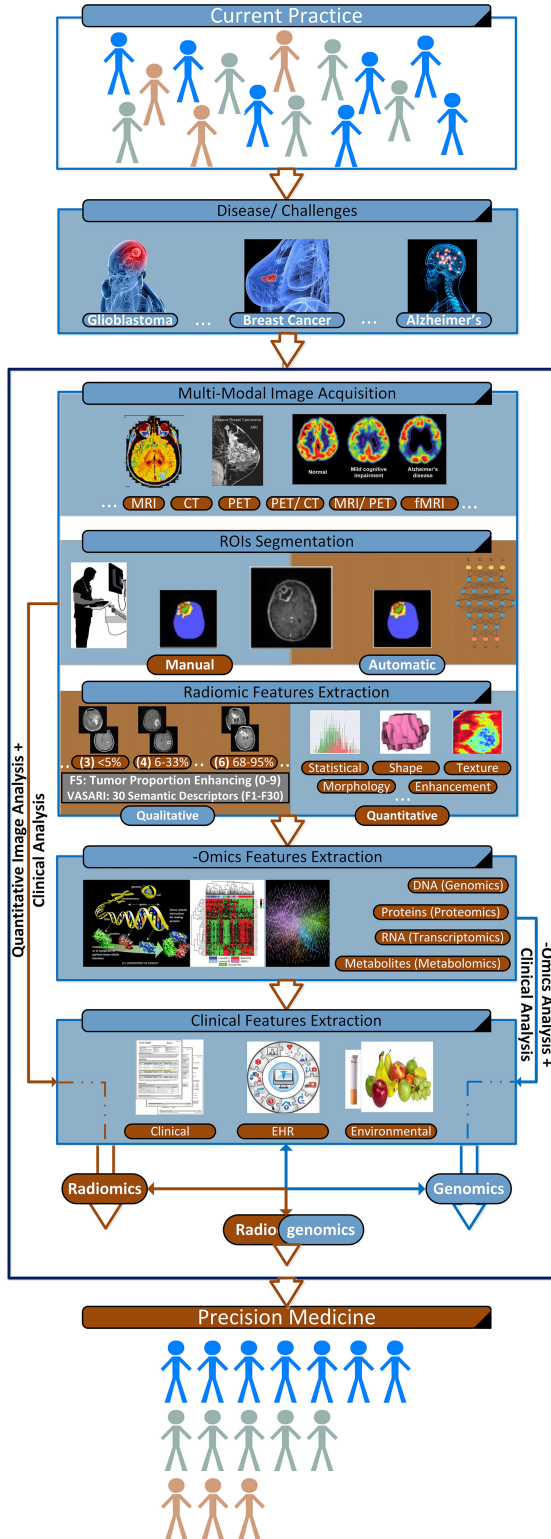


**Fig. 1.** Radiogenomics System Diagram: An abstract system diagram that depicts the benefits of adopting radiogenomics methods for precision medicine. Based on the disease, we use the corresponding (multi-)modal imaging approach. Following manual and/or automatic segmentation of the clinically important regions, quantitative and/or qualitative features are then extracted. Radiogenomics investigate the relationships between imaging and genomic features and how radiomics and genomic signatures are associated with clinical outcomes. Radiomics is focused on characterizing the relationship between quantitative (multi-modality) imaging and clinical features.

learning methods train complex classifiers to achieve superior classification results. Unfortunately, it is often hard to understand how deep learning hidden layers operate. This is especially true when deep learning methods are used with raw images and are thus tasked to also perform feature extraction. As shown in Fig. 1, our paper focuses on the specific clinical features used in clinical applications. Furthermore, we also summarize the use of well understood biostatistical methods as well as segmentation methods for both visualizing the results and driving clinically relevant analysis. Overall, clinical value amidst the increasing complexity of big data analytics goes through explainable, extensible, and reproducible research (see Section II-C).

Large-scale datasets for radiogenomics research are currently available through open research data initiatives, such as the Cancer Imaging Project (CIP) [27], [28] and the Alzheimer’s Disease Neuroimaging Initiative (ADNI) [29]. These datasets provide multi-modal imaging, genomic, and clinical data. Here, we consider CIP and ADNI as case studies with the expectation that methods developed for these datasets will find wider applications in other diseases as well.

The rest of the paper is organized as follows: In Section II, we briefly review radiogenomics studies’ methodological approaches and discuss the challenges associated with quantitative imaging in the big data era with a deep learning flavor. Next, in Section III and Section IV, we provide case studies of state-of-the-art radiogenomics research in cancer and Alzheimer’s disease, respectively that highlight the profound impact that such research can have on precision medicine. Finally, Section V provides discussion and concluding remarks.

## II. QUANTITATIVE IMAGING IN THE RADIOMICS ERA

This section starts with a brief methodological overview of radiomics and radiogenomics studies, followed by a discussion of quantitative imaging from a big data angle. It then highlights key challenges associated with the analysis of large-scale, multi-modality medical image databases that are typically used in such studies, towards the uptake of radiogenomics research in clinical practice. It concludes with presenting the emerging uses of deep learning methods.

### A. A brief Methodological Overview

Radiomics research uses quantitative imaging methods to associate multi-modal image features to clinical outcomes. Radiogenomics research extends radiomics scope by investigating the association of these features to –omics analysis, therefore creating imaging phenotypes as surrogate, non-invasive biomarkers. Moreover, by creating radiogenomics signatures. That is, the development of joint models leveraging imaging and genomic features that better describe and correlate to clinical outcomes (features), and as a result can be used for enhancing prognosis, diagnosis, and treatment response. Naturally, radiomics and radiogenomics studies share the same methodological concepts as depicted in the abstract radiogenomics system diagram in Fig. 1.

Standardizing image acquisition is of primary essence in the big data landscape as discussed in the following subsections and the first step towards achieving reproducible research by design

**TABLE I**  
DEEP LEARNING BASED RADIOGENOMICS AND RADIOMICS STUDIES

|                      | YEAR                                       | DISEASE           | IMAGING DATA | PATIENTS | METHOD   | DL FRAMEWORK          | SEGMENTATION     | DESCRIPTION  |
|----------------------|--|-------------------|--------------|----------|--|-----------------------|------------------|--|
| <b>RADIOGENOMICS</b> | 2015-Error!<br>Reference source not found. | Esophageal Cancer | PET          | 107      | 4 convolutional and 4 max-pooling layers                                 | N/A                   | Bespoke software | Predict neoadjuvant chemotherapy treatment response              |
|                      | 2017-Error!<br>Reference source not found. | LGG               | MRI          | 151      | 6 convolutional and 1 fully connected layers                             | N/A                   | ✓                | Predict mutation status of IDH1                                  |
|                      | 2017-Error!<br>Reference source not found. | GBM               | MRI          | 112      | Transfer learning  | CAFFE                 | 3D Slicer        | Overall survival prognostic signature and patient stratification |
|                      | 2017-Error!<br>Reference source not found. | LGG               | DTI-MRI      | 79       | Single layer neural network  | N/A                   | ITK-Snap         | Predict mutation status of IDH1                                  |
|                      | 2017-Error!<br>Reference source not found. | GBM               | MRI          | 155      | ResNet (18, 34, and 50 layers)   | Keras                 | ✗                | Predict methylation status of MGMT                               |
|                      | 2017-Error!<br>Reference source not found. | Breast Cancer     | DCE-MRI      | 270      | Training, transfer learning, off the shelf features                      | CAFFE                 | Manual           | Discriminate between Luminal A and other cancer subtypes         |
|                      | 2018-Error!<br>Reference source not found. | LGG               | MRI          | 201      | 34 layer residual network (based on ResNet)                              | Keras (on TensorFlow) | 3D Slicer        | Predict IDH glioma mutation status                               |
|                      | 2018-Error!<br>Reference source not found. | LGG and GBM       | MRI          | 135      | 50 layer residual network (based on ResNet)                              | Keras                 | ITK-Snap         | Predict ATRX mutation status                                     |
| <b>RADIOMICS</b>     | 2017-Error!<br>Reference source not found. | Bladder Cancer    | CT           | 82       | Training and transfer learning, cuda-convent-5 convolutional layers      | N/A                   | AI-CALS          | Predict treatment response (complete vs non-complete)            |
|                      | 2017-Error!<br>Reference source not found. | N/A               | CT           | 48       | ConvNet transfer learning (3 convolutional and 1 fully connected layers) | ConvNet               | Vitrea           | Predict patient longevity (5-year mortality)                     |

N/A: Not Applicable, PET: Positron Emission Tomography, CT: Computer Tomography, MRI: Magnetic Resonance Imaging, DTI-MRI: Diffusion Tensor Imaging MRI, DCE-MRI: Dynamic Contrast Enhancement MRI, LGG: Lower Grade Glioma, GBM: Glioblastoma, ATRX: alpha-thalassemia/mental retardation syndrome X-linked.

[30], [31]. Pre-processing facilitates the procedures installed that will enable joint processing of large-scale data and will in-turn produce interpretable measurements, especially in view of multi-institutional collaboration involving different medical equipment and protocols. Typical pre-processing tasks involve de-identification [32], image correction (normalization), skull stripping (e.g., for brain cancer and Alzheimer's disease), and registration (see [33] for further discussion).

Next, the goal is to determine the Diagnostic Region of Interest (ROI). Thus, accurate segmentation methods are essential in determining precise ROIs. The latter is further depicted by the *brain tumor image segmentation* (BraTS) challenge described in Section II-C below [34]. A number of segmentation algorithms have been proposed for this purpose as summarized in Tables I, III.A, IV.A, and V. However, manual experts' consensus annotations dominate the majority of radiomics and radiotherapy studies, especially during models training [30]. Here, it is important to note that the segmented regions are largely aligned and

correspond to clinical assessment, as for example the VASARI feature set for glioblastoma described in Section III.B (see also Fig. 2).

Once the ROI labels have been derived, image features are extracted from the segmented regions. Image features depend on the imaging modality and characteristics of the specific disease. For example, in breast cancer, these features can be broadly categorized into statistical, shape, texture, morphological, kinetic and enhancement features [35]. Feature extraction follows feature selection and then classification (predictive) models are constructed using the selected features and the desired (clinical) outcome according to the investigated hypothesis.

Here, we note that radiotherapy case studies to be discussed in Sections III and IV exploit already derived genomic analysis features. The availability of such open-source databases allows research teams to focus their efforts on the quantitative imaging methods. For instance, the ADNI database facilitates openly available genome wide association studies (GWAS)

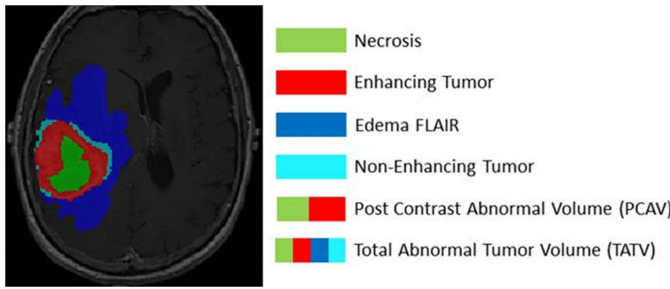


**Fig. 2.** VASARI- based diagnostic ROIs segmentation for GBM. VASARI defines 30 semantic descriptors for which a qualitative score is provided by medical experts. The depicted GBM tumor automated segmentation was performed using the BraTumIA software [111] (figure extracted from [112]).

data. Likewise, The Cancer Imaging Archive (TCIA) provides matched genetic data and associated features from The Cancer Genome Atlas (TCGA), that can be downloaded and/ or pulled and processed using open-source software such as the TCGA-Assembler [36]. –Omics analysis is further facilitated by state-of-the-art tools and methods, including gene set enrichment analysis (GSEA) [37] for studying differential gene expressions (e.g., RNA and protein expressions, mutations, transcriptional activities, etc.) and ingenuity pathway analysis (IPA) [38] for investigating pathway and network analysis (e.g., upstream/ downstream regulation, networks interaction, etc.). In that sequence, disease-based biological processes knowledge is generated, profiles are constructed, and potential biomarkers are discovered.

Positive and/ or negative association to clinical and –omic features is typically performed using well-known statistical methods. Such methods include the Spearman rank correlation coefficient, the Pearson’s product moment correlation coefficient, and the Fisher’s exact test. Then, radiogenomics predictive models can be build using a number of statistical and shallow or deep machine learning algorithms [39]. Linear and logistic regression are often employed as depicted in **Tables III.B**, **IV.B**, and **VI**. Models training and validation use well-established cross-validation methods while performance is often summarized using the area under the receiver operating characteristic (ROC) curve (AUC). Survival models typically employed in cancer related radiogenomics studies are based on Kaplan-Meir estimator and Cox regression algorithms [40].

### B. Quantitative Imaging from a Big Data Perspective

Medical images contain information about the underlying pathophysiology that can be used for: (i) tumor phenotyping, (ii) increasing diagnosis precision, (iii) assessment of disease prognosis, and prediction of treatment outcome and/ or therapy response, and (iv) monitoring of disease status. In what follows, we present a Big Data perspective of quantitative imaging based on *volume*, *velocity*, *variety*, *veracity*, *variability*, *value*, and *visualization*.

**Volume:** An average US hospital was estimated to generate more than 665 Terabytes annually in 2015 [41]. Together with medical video, medical images dominate volume requirements

[42], [43]. Indicatively, picture archiving and communication systems (PACS) account for most of the generated data, with an annual growth rate between 20-40% [41].

**Velocity:** Velocity is primarily due to high-throughput technologies and infrastructure, multi-modal image acquisition exploiting availability of affordable equipment, and the ageing population (including chronic diseases) [17]–[21].

**Variety:** Variety comes from the use of different medical image modalities. Non-exhaustive examples include Mammograms (~150 MBs), Computer Tomography (CT), 3D CT Scan (~1 GB), Magnetic Resonance Imaging (MRI), 3D MRI (~~150 MB), functional MRI (fMRI), Positron Emission Tomography (PET), and recently new MRI/PET and PET/CT images [5]–[7], [44]. Importantly, there is a strong variety among image acquisition protocols and employed device specifications that generate even more variations. Here, there is a clear need for standardization in both the acquisition (1st) and (pre) processing (2nd), to facilitate multi-institutional collaboration for large-scale database creation and analytics.

**Veracity:** In healthcare systems, veracity is associated with the clinical quality of the data. Medical imaging data coming from uncontrolled environments with inadequate acquisition information and incomplete clinical data, are often of limited clinical significance in follow-up big data analysis studies. On the other hand, data coming from controlled, clinical trials, often tend to produce data that are more suitable for large-scale studies that investigate medical image features [18].

**Variability:** A large portion of available medical images lack any follow up longitudinal examinations and/or are scattered across healthcare datacenters. The latter, makes it difficult to collect and describe in a uniform manner or link to the appropriate clinical knowledge that will drive further analytics towards investigating new image biomarkers.

**Value:** Preventive, predictive, personalized, and participatory (P<sup>4</sup>) health will pave the way towards informed decision making and interventions that can improve quality of care while reducing associated healthcare expenditures.

**Visualization:** Here, the challenge is to provide personalized and meaningful information via role assignment to different stakeholders. Semantically interconnecting the generated metadata with other healthcare data using conceptually relevant ontologies for further analysis and new workflows investigation and display is of primary importance.

### C. Radiogenomics Challenges From a Big Data Analytics Perspective

Big data programming models (e.g., [19]–[22]) can provide effective methods for analyzing data associated with quantitative imaging. Often, big data programming models are confused as the vehicle that will -by leveraging computationally intensive tasks only- automatically lead to new knowledge creation. Indeed, computational efficiency can facilitate new knowledge that results from the wider adoption of extensive experimentation [45]. Clearly then, the true novelty does not come from computational efficiency itself, but rather from the fact that big data

analytics allow for different hypothesis testing, both clinically and algorithmically, hence allowing methodological and data (clinical) workflow advances. Moreover, the latter highlights the true potential for precision medicine, as research studies involving large cohorts have been shown to reduce uncertainties associated with findings relying on limited datasets, providing for more robust outcomes [46].

Central to the success of quantitative imaging using big data technologies field, is the construction of well curated open-source healthcare datasets that will consist of heterogeneous multi-level data, such as the ones described in Section III and IV. The objective is to allow for *reproducible*, *extensible*, and *explainable* research studies. Toward this direction, FAIR guiding principles set the foundations for *fairness* in both human and machine driven related activities that pertain to (meta) data manipulation, establishing a set of recommendation that aid in constituting (meta) data findable, accessible, interoperable, and reusable (FAIR) [47].

*Reproducibility* benefits from the sharing of common data acquisition protocols and methods per investigated data [48], relies on *Integrating the Healthcare Enterprise* (IHE) profiles for data storage and communication, and the definition of semantic descriptors for resulting metadata manipulation [49]. Instrumental to this process, is semantic annotation of diagnostic ROIs that guide image feature extraction. At the same time, proper documentation of the selected clinical cohorts available in the datasets and the applied processing steps is of primary essence.

*Extensibility* objectives are twofold. First, to accommodate (new) data entry in a standardized fashion that will allow increasing the statistical power of the performed studies. Second, to effectively store and post-process resulting metadata, in order to facilitate knowledge transfer between studies, and avoid replicating already known results.

In terms of *explainable* research, this is largely attributed to aforementioned objectives, linked with proper visualization of not only the results, but also the investigated workflows and methods, visualizing intermediate results, by generating appropriate descriptive techniques based on metadata. Additional challenges include legal, privacy, and data ownership that need to be effectively addressed [50], [51].

Moreover, the grand challenges associated with biomedical image analysis range from the need of developing methods for specific tasks (e.g., image segmentation and classification) to their associations with disease prediction and evolution (e.g., [52]). The challenges are aligned with the aforementioned objectives of generating FAIR data and working towards reproducible, extensible, and explainable solutions. In view of the presented case studies in Section III, one can identify the *combined radiology and pathology classification* and the *brain tumor image segmentation* (BraTS) challenges that relate to lower grade glioma (LGG) and Glioblastoma (GBM) brain cancers, respectively, or the computational precision medicine challenge, all of which utilize datasets that reside in TCIA [53]. Additionally, with respect to the case study presented in Section IV, the *Alzheimer's disease prediction of longitudinal evolution* (TADPOLE) challenge utilizes the ADNI database [54].

#### D. Deep Learning

The early growth of Deep learning methods greatly benefited from the availability of ImageNet, a big data source, associated with the Large Scale Visual Recognition Challenge (ILSVRC) [55]. A sequence of deep learning architectures were presented in AlexNet [56], GoogleNet [57], VGGNet [58], SqueezeNet [59], and ResNet [60]. The growth of these architectures has been also facilitated by the introduction of high level open source deep learning frameworks such as Caffe2 [61], PyTorch [62], Keras [63], and earlier Theano [64] that utilize dedicated data science libraries, namely TensorFlow [65] and Microsoft Cognitive Toolkit (CNTK) [66]. These deep learning frameworks have been widely adopted due to their use in well-documented interfaces to Python and MATLAB. Furthermore, these frameworks provide heterogeneous computing implementations [67] (e.g., CPU-GPU), and are also available through platform-as-a-service (PaaS) cloud services (e.g., Nvidia GPU Cloud supporting Nvidia DIGITS [68], Amazon Elastic Compute Cloud (EC2), Google Cloud, Microsoft Azure) that also facilitate an off the shelf solution to the computationally intensive processes that are often involved.

The rapid growth of deep learning methods is primarily attributed to the fact that they tend to provide significant improvements in classification accuracy. Unfortunately, accuracy comes at a high prize. They are hard to train and even harder to understand how they work. Yet, research and development of deep learning methods is expected to grow substantially [69]. Indicatively, over the past two years, there have been more than 300 studies in the development and application of deep learning methods [70]. Recent deep learning for medical image applications range from image classification to object or lesion detection and localization, image segmentation and image registration [70]–[73]. The latter studies, can be used in computer assisted diagnosis (CAD), content based image retrieval (CBIR), and case-based image query systems. Such systems in clinical practice are expected to have a catalytic impact in precision medicine.

The majority of these studies are associated with convolutional neural networks (CNNs) where the network learns convolutional kernels that can better classify the input into different categories. Wider adoption has also benefited from the use of transfer learning methods [72]. Transfer learning reduces the need for large training time and large datasets by using the lower layers of pre-trained CNNs. Here, the assumption is that the lower layers can be used for feature extraction for new problems. The lower-layers can be frozen and hence learning will only be required to adapt the upper-layers with much fewer parameters [73]. The approach is effective provided that the pre-trained system was used in classification problems that are closely associated to the investigated new problem.

Nevertheless, there are very few studies that use deep learning methods in radiomics and radiogenomics research. As depicted in Table I, most studies focus on cancer research [74]–[82]. More precisely, three studies investigated the prediction of IDH1 mutation status for Lower Grade Glioma (LGG) [75], [77] and low and high grade glioma [80], respectively, while another

**TABLE II**  
THE CANCER IMAGING ARCHIVES (TCIA) RESEARCH GROUPS

| TCGA RESEARCH GROUP   | CANCER TYPE                                   | MODALITY                              | NO. PATIENTS | NO. IMAGES | SIZE (GB) |
|-----------------------|---|---------------------------------------|--------------|------------|-----------|
| 1 BLADDER PHENOTYPE   | UROTHELIAL BLADDER CARCINOMA (BLCA) [90]      | CT, CR, MR                            | 106          | 78,429     | 40.1      |
| 2 BREAST PHENOTYPE    | BREAST INVASIVE CARCINOMA (BRCA) [91]         | MR, MG                                | 139          | 230,167    | 88.1      |
| 3 GLIOMA PHENOTYPE    | GLIOBLASTOMA (GBM) [92]                       | MR                                    | 262          | 481,158    | 73.5      |
|                       | LOWER GRADE GLIOMA (LGG) [93]                 | CT, MR                                | 199          | 241,183    | 42.8      |
| 4 HEAD-NECK PHENOTYPE | HEAD-NECK SQUAMOUS CELL CARCINOMA (HNSC) [95] | CT, MR, PET, RTDOSE, RTPLAN, RTSTRUCT | 192          | 247,398    | 108.3     |
| 5 RENAL PHENOTYPE     | KIDNEY RENAL CLEAR CELL CARCINOMA (KIRC) [96] | CT, MR                                | 267          | 192,581    | 91.6      |
| 6 OVARIAN PHENOTYPE   | OVARIAN SEROUS CYSTADENOCARCINOMA (OV) [97]   | CT                                    | 143          | 53,662     | 28.3      |

CT: Computed Tomography; CR: Computed Radiography; MR: Magnetic Resonance; MG: Mammography; PET: Positron Emission Tomography; RTDOSE/RTPLAN/ RTSTRUCT: DICOM Radiotherapy Modules.

**TABLE III.A**  
TCIA BRCA GROUP RADIOMICS STUDIES COMMON MATERIAL AND METHODS

|   |   |                        |                      |
|---|---|------------------------|----------------------|
| QUANTITATIVE IMAGING/ RADIOMIC FEATURES | Dynamic Contrast Enhanced (DCE) MRI, T1-weighted DCE MRIs <sup>1</sup><br>38 Radiomic Features into six MRI phenotype categories: size (4), shape (3), morphology (3), enhancement texture (14), kinetic curve (10), enhancement-variance kinetic (4) |                        |                      |
| CLINICAL DATA                           | Estrogen Receptor (ER), Progesterone Receptor (PR), Human Epidermal Growth Factor Receptor 2 (HER2), Tumour Stage I, II, III, Lymph node metastasis, 2.5: Molecular subtype (normal-like, luminal A, luminal B, HER2-enriched, and basal-like)        |                        |                      |
| SEGMENTATION                            | Fuzzy c-means (FCM)-based [106]   | Genomic Data Retrieval | TCGA-Assembler [105] |

study addressed the prediction of MGMT methylation status for Glioblastoma (GBM) [78]. Moreover, radiogenomics and radiomics approaches were employed towards the prediction of overall survival for patients with GBM in [76] and non-disease specific subjects in [83], respectively. Discrimination between Luminal A and other breast cancer subtypes was demonstrated in [79], while radiomic features for bladder cancer treatment response prediction was performed in [82]. Notably, besides [75] and [74], [77] (the latter two using a neural and a convolutional neural network, respectively), all other studies exploited transfer learning approaches over the segmented tumor region. Segmentation was typically performed either manually or semi-automatically, although examples of using the whole image to train a deep neural network exist [78], [81]. In [81], classification superiority of deep learning in distinguishing between no tumor, ATRX mutation, and no ATRX mutation, for LGG and GBM, compared to classical machine learning (support vector machines (SVM)) was demonstrated (note: segmentation only employed for SVM). Importantly, automatic segmentation approaches exploiting deep learning architectures [34], [84] are crucial in streamlining large-scale image analytics studies [70].

Undoubtedly, research in deep learning applications and methods is expected to grow, especially in relation to the research areas that are presented in the following sections. In that sequence, deep learning methods flourish, with comparable success to imaging applications, across the spectrum of healthcare data, such as EHR [85], [86], genomic [87], [88], and physiological parameters [89] data processing.

### III. CASE STUDY I: CONNECTING CANCER PHENOTYPES TO GENOTYPES

In response to the ever increasing scientific community demands for heterogeneous multi-level data sharing and driven by notable research discoveries that underpin inter-institutional

and inter-disciplinary research, TCIA is building a publicly accessible database, implementing the FAIR principles, providing clinical diagnostic images matched to subjects of TCGA. The CIP TCGA Radiology Initiative aspires to establish new frontiers on connecting cancer phenotypes to genotypes, enriching genetically analyzed tissue cases with the corresponding clinical images for the more than 20 cancer types found in TCGA. Currently, six research groups have been formed investigating different tumor types as depicted in Table II. In what follows, a brief overview of novel retrospective studies that were carried out by TCIA breast and glioma phenotype groups, having published the most significant share of TCIA research papers, is presented. It is reasonable to expect that tools and methods used in these papers will be applicable to different cancer subtypes and diseases as well. Notably, a significant portion of TCIA analysis results, including presented studies from Tables III and IV below, are further stored and made available to the research community, augmenting the primary datasets [98]. Preliminary renal phenotype group's findings appear in [99].

#### A. Breast Invasive Carcinoma

Invasive Lobular Carcinoma (ILC) is the 2nd most frequently diagnosed invasive breast cancer (between 10%–15% of all cases) and has been identified both clinically and molecularly as a distinct disease [91]. Based on the joint TCIA and TCGA datasets, research hypotheses investigated radiogenomics approaches linking radiomics features to genomic profiles, molecular subtypes, and recurrence scores as well as joint radiogenomics signatures for improved prediction of clinical outcomes [13]. Methods are tabulated in Tables III.A and III.B.

A total of 91 patients with clinical images, matched genomics profiles, and associated clinical data from the TCIA and TCGA datasets, respectively, were involved in studies [35], [100], [101], [104], while the sample size was 84 in [103]. The

**TABLE III.B**  
TCIA BRCA GROUP RADIOGENOMICS STUDIES DESCRIPTION

| YEAR<br>PATIENTS<br>(RADIOLOGIST)<br>No. | GENETIC DATA   | BIOSTATISTICAL METHODS   | DESCRIPTION   |
|--|--|--|---|
| 2015-[35]<br>91 (3)                      | <b>Features:</b> 144:<br><b>Copy Number (CN):</b> 70<br><b>Gene Expression (GE):</b> 40<br><b>DNA methylation (ME):</b> 4                                      | T-test (correlation), LASSO logistic regression (radiogenomic predictive models), Leave-one-out cross validation (model train/ test), ROC/AUC (validation)   | +Radiomic size features significantly associated with tumor stage<br>+Genomic features predictive of ER/PR and HER2 (lesser extend) status<br>-Radiogenomics approach did not yield increased predictive performance  |
| 2016-[100]<br>91 (3)                     | Not considered   | Pearson Correlation (CEIPs correlation), Leave-one-out cross validation (model train/ test 2-CEIP models), ROC/AUC (validation)  | +Tumor size predictive of pathological tumor stage as in [35]<br>+Enhancement texture homogeneity linked to tumor stage<br>+Homogeneity feature associated to larger tumor lymph node status whereas irregularity feature to smaller lymph node status  |
| 2015-[101] <sup>a</sup><br>91 (3)        | <b>GE:</b> 20531 genes<br><b>CN variations:</b> 19950 genes<br><b>miRNA expressions:</b> 1046<br><b>Protein expressions:</b> 142<br><b>Mutated genes:</b> 3734 | GSEA (pathways association), Linear regression (miRNA association), APC (tumor clustering), Fisher's exact test (tumor partitions association to tumor stage and receptor status)                    | +Transcriptional activities of pathways associated to tumor size, blurred tumor margin, and irregular tumor shape features<br>+miRNA expressions linked to tumor size and enhancement texture<br>+Insights to genetic mechanisms that guide tumor development   |
| 2016-[103]<br>84 (3)                     | <b>Multigene assays:</b><br>MammaPrint,<br>Oncotype DX,<br>and PAM50   | Multiple linear regression with stepwise feature selection (multigene assay classification association), Leave-one-out cross validation (model train/ test), ROC/AUC (validation)                    | +Radiomic features association to multigene assay classification based on (a) subtype and on (b) subtype and proliferation<br>+Distinguishing between good and poor prognosis of high and low-to-medium breast cancer recurrence risk<br>+Investigated associations yielded moderate to good correlations<br>+Tumor size and enhancement texture, the latter potentially linking to tumor heterogeneity linked to breast cancer relapse |
| 2016-[104]<br>91 (3)                     | Not considered   | Stepwise leave-one-out cross validation & Linear discriminant analysis (predictive molecular classification models), Kendall coefficient tau-b(molecular subtypes association), ROC/AUC (validation) | +Quantitative imaging features predictive of molecular classification, distinguishing between ER+ vs ER-, PR+ vs PR-, HER2+ vs HER2-, and TN vs others<br>+Larger tumor size and higher contrast enhancement heterogeneity associated with more aggressive cancers<br>+Entropy enhancement feature linked to molecular subtypes   |

<sup>a</sup>Data extracted from all genetic pathways found in the Kyoto Encyclopedia of Genes and Genomes (KEGG) [102].

ER: Estrogen Receptor; PR: Progesterone Receptor; HER2: Human Epidermal Growth Factor Receptor 2; miRNA: microRNA; TN: Triple Negative.

TCGA assembler software was used to extract analysis results and clinical data from the TCGA [105]. In all studies, consensus delineations from 3 expert radiologists defined the tumor location on MRI images, which were later segmented using a fuzzy c-means algorithm [106]. Radiomics features stemming from T1-weighted Dynamic Contrast Enhancement (DCE) Magnetic Resonance Imaging (MRI) were classified in the following six phenotype categories: (i) *size*, (ii) *shape*, (iii) *morphology*, (iv) *enhancement texture*, (v) *kinetic curve assessment*, and (vi) *enhancement-variance kinetics*, amounting 38 distinct features. The reader is referred to [35] for a detailed radiomic features description. Primary clinical data included tumor stage, lymph node metastasis, estrogen receptor (ER), progesterone receptor (PR), and human epidermal growth factor receptor 2 (HER2). Molecular subtype classification was investigated in [104].

**1) Key Clinical Outcomes:** Radiomic size features were significantly associated with tumor stage as depicted in [35], [100], and [104]. In fact, all four size features, namely lesion volume, effective diameter, surface area, and maximum linear size, were positively associated with tumor stage in [35], with effective diameter and surface area being the most robust features in discriminating between tumor stages [35], [100]. Enhancement texture homogeneity was also found to be positively associated with tumor stage, suggesting that larger, heterogeneous tumors are potentially linked to more aggressive cancers [104] with higher probability of recurrence [103]. Radiomic features (size, enhancement texture, and kinetic curve phenotypes) predictive

ability between poor and good prognosis with respect to multi-gene assay recurrence scores of MammaPrint (good vs poor), Oncotype DX (low & medium vs high), and PAM50 ROR-S and ROR-P (low & medium vs high) yielded moderate correlations of 0.88, 0.76, 0.68, and 0.55, respectively [103]. Enhancement texture maximum correlation coefficient was negatively associated with all four multigene assays. Moreover, enhancement texture homogeneity feature [100] was further associated with larger lymph node status while irregularity feature was linked to smaller lymph node status.

Interestingly, quantitative imaging phenotypes of size, shape, and enhancement texture have performed relatively well in predicting clinical receptor status, namely ER+ vs ER- (ROC curve value 0.89), PR+ vs PR- (0.69), HER2+ vs HER2- (0.65), and TN vs others (0.67), that can be exploited towards forming prognostic indicators [104]. Statistically significant difference was documented for the aforementioned radiomic features used for molecular subtyping between Normal-like, Luminal A, Luminal B, HER-enriched, and Basal-like.

Perhaps the most comprehensive radiogenomic study in BRCA group is reported in [101]. Genetic pathways and quantitative imaging phenotypes equaled 1,103 associations encompassing all investigated radiomic features. A total of 45 associations were documented between mutated genes and radiomic features, with kinetic curve assessments and enhancement texture features summing 37. Importantly, miRNA expressions were significantly associated with size and enhancement texture

**TABLE IV.A**  
TCIA GBM GROUP RADIOMICS STUDIES COMMON MATERIAL AND METHODS

|                    |   |                        |              |
|--------------------|---|------------------------|--------------|
| MATERIAL           | Pre- & post- contrast enhanced axial T1-weighted (T1W) MRI, axial T2-weighted (T2W) fluid-attenuated inversion recovery (FLAIR) images  |                        |              |
| VASARI FEATURE SET | VASARI features: 30, categorized into (i) non-enhanced tumor, (ii) contrast-enhanced tumor, (iii) necrosis, and (iv) edema<br>VASARI features describe (a) tumor location, (b) tumor substance and boundary morphology, (c) alterations in the vicinity of the tumor and (d) the tumor resection extend |                        |              |
| SEGMENTATION       | 3D Slicer, ePAD, ClearCanvas, NordicICE   | GENOMIC DATA RETRIEVAL | TCGA Website |

phenotypes but not with shape, morphological, and enhancement variance kinetics features. Enhancement texture (17), size (10), and morphological (9) features were further linked to protein expressions.

### B. Glioblastoma (GBM)

Glioblastoma is the most lethal brain cancer, associated with low median overall survival rates. According to the 2016 WHO classification of Central Nervous System Tumors, glioblastomas can be categorized into (i) *IDH-wildtype* (primary, approximately ~90% of all cases, median survival between 9.9–15 months), (ii) *IDH-mutant* (secondary, approximately ~10% of all cases, median survival between 24–31 months), and (iii) *not otherwise specified (NOS)*, for tumors that a full IDH evaluation is not feasible [107]. GBM has been systematically studied by the TCGA in an attempt to map the genomic landscape of both glioblastoma [92] and lower grade glioma [93] tumors. In what follows, key radiogenomics studies of TCGA and TCIA matched subjects are presented, extending the discussion of [94]. Primary knowledge advancement is further described in **Table IV.B**.

Toward this direction, the Visually AcceSable Rembrandt (VASARI) project defined a controlled terminology and rating schema of the 30 most prevailing subjective MRI features that describe malignant gliomas. The objective was to establish a common reference schema that would allow reproducibility and extensibility of results across institutions in a clinically meaningful and biologically relevant manner, underpinning explainability [108]–[110]. The VASARI feature set was developed by expert neuroradiologists and its 30 features can be categorized with respect to (i) *non-enhanced tumor*, (ii) *contrast-enhanced tumor*, (iii) *necrosis*, and (iv) *edema*. The aforescribed classes describe the tumor location, its substance and boundary morphology, as well as any alterations in the vicinity of the tumor and the tumor resection extend. The VASARI features guide appears in [109] while a visual example is depicted in **Fig. 2**, generated using an automatic tumor segmentation software termed BraTumIA [111], [112]. Recently, automatic segmentation labels and manual annotations of pre-operative MRI images of both GBM and LGG TCGA datasets has been released, accompanied by a rich radiomic feature set [33]. Quantitative imaging (radiomic) features that are considered in the following studies were based on pre- and post- contrast enhanced axial T1-weighted (T1W) MRI for segmenting the necrosis and enhancement ROIs as well as axial T2-weighted (T2W) fluid-attenuated inversion recovery (FLAIR) images for defining the edema ROI [113] (see also **Table IV.A** and **Fig. 2**).

**1) Key Clinical Outcomes:** As tabulated in Table IV under biostatistical tools, all studies involved survival analysis. In [114], key findings reported that while female patients had significantly lower volume of necrosis compared to men and hence significant survival advantage, when it came to high volume of necrosis, female patients had notably lower survival than male patients. Moreover, cell death was associated with TP53 activity and MYC, in male and female patients, respectively, linking sex-specific molecular signatures to oncogenesis and cell death.

In [116], 3 enhancement features were associated with overall survival. Good prognosis was associated with a (i) low value of radial distance variance, describing enhancement border irregularity, (ii) sharp enhancement border (contrary to smooth border), and (iii) low edge sharpness blurriness value. In agreement with results of previous studies, key findings in [119] verified the association between the degree of contrast enhancement and the length of the major axis of the lesion with overall survival. Significant associations between imaging, genomic, and clinical (age at initial diagnosis, gender, ethnicity, race, radiation therapy, chemotherapy, hormonotherapy, and immunotherapy) features with respect to overall survival were documented in [118]. Results reported that proportion of tumour contrast enhancement, HRAS copy number variation, and chemotherapy, gave the best results, respectively. Adopting an integrative radiogenomics approach incrementally outperformed individual biomarkers in prediction accuracy.

Radiogenomics towards forming unique prognostic indicators was also assessed in [117]. Considering imaging (morphological and physiological) and genomic features analysis, correlation to overall and progression-free survival was conducted. Results showed that poor survival was associated with patients having high relative cerebral blood volume ( $rCBV_{ner}$ ) of the non-enhancing region (NER) and NER crossing the midline. High  $rCBV_{ner}$  and wild-type epidermal growth factor receptor mutation was also associated with low survival. High  $rCBV$  (contrast enhanced  $rCBV_{max}$  and  $rCBV_{mean}$  and non-enhanced  $rCBV_{ner}$ ) values were also associated with poor overall survival in [120]. Overall,  $rCBV_{ner}$  was identified as an independent prognostic biomarker of survival. Similarly,  $rCBV_{max}$  was reasoned as a distinct predictor in [120].

Two phenotype classes based on the presence or the absence of invasive imaging descriptors guided by VASARI qualitative tumor assessment was performed in [115]. Results showed that patients in the 1st class that combined ependymal invasion (EP) and deep white matter tracts (DWMT) were associated with decreased survival, as opposed to patients belonging in the 2nd class, in the absence of invasive imaging features. In terms of top canonical pathway, mitochondrial dysfunction was associated with the documented invasive imaging features of the 1st

**TABLE IV.B**  
TCIA GBM GROUP RADIOGENOMICS STUDIES DESCRIPTION

| YEAR<br>PATIENTS<br>(RAD.) NO.                                   | GENETIC DATA  | BIOSTATISTICAL METHODS  | DESCRIPTION   |
|--|---|---|---|
| 2014-[114]<br>99 (2) <sup>a</sup>                                | <b>Total genes:</b> 13628<br><b>micro RNAs:</b> 555<br>(Affymetrix level 1 mRNA and Agilent level 1 microRNA) | Kaplan-Meir (survival), Excel, JMP, R <sup>2</sup> statistical packages (correlation), CMS (significance probing), IPA (pathway), CMAP (functional connections)                               | +GBM cell death was associated with sex-specific molecular mechanisms<br>+ Men had higher volume of necrosis than female patients for equivalent active tumor cells<br>+Significant survival advantage in women with low volume of necrosis   |
| 2014-[115]<br>104 (7)  | As above  | As above + proportional hazard regression   | +EP and DWMT involvement and tumor extension across the midline GBM imaging phenotypes were associated to decreased survival<br>+Classification into Class A (invasive phenotypes) and Class B (non-invasive) better predicted survival than tumor size and subject age<br>+Class A linked to mitochondrial dysfunction; MYC oncogene; NFKBIA   |
| 2014-[116]<br>55 (1)   | <b>Gene expression,</b><br><b>DNA methylation,</b> and<br><b>CN</b> into coexpressed gene modules             | Amareto, elastic net linear regression, GSEA, intra class correlation coefficient (ICC), hierarchical clustering, Cox regression (survival), Spearman correlation                             | +3 enhancement imaging features correlate to survival; 77 associations between quantitative imaging and qualitative VASARI features; 7 imaging features linked to molecular subgroups<br>+Prognostic radiogenomic maps suggest the linkage of tumor phenotypes to underlying key biological pathways  |
| 2014-[117]<br>45 (3)   | <b>cBIO Genomics Portal,</b><br><b>Mutations</b> (4): EGFR, PTEN, TP53, PDGFRA                                | Analysis of Variance (correlations), Cox regression, Kaplan-Meier, Random Forests – R (survival)  | +NER imaging biomarkers can increase prognosis non-invasively<br>+(a) NER crossing the midline and high rCBV <sub>ner</sub> , and (b) high rCBV <sub>ner</sub> and wild-type EGFR mutation were associated with decreased survival  |
| 2015-[118]<br>102 (6)  | <b>Gene expression,</b><br><b>Total genes:</b> 17787<br><b>Mutations:</b> 10<br><b>CN genes:</b> 14           | GSEA (pathway), Univariate Cox model analysis (association), Cox regression (survival), AIC (model robustness), AUC (validation)  | +A combinatorial biomarker consisting of clinical factors (chemotherapy), imaging features (proportion of enhancing tumor), and genomics (HRAS copy number variation) was found to best predict survival of patients with GBM compared to individual survival models  |
| 2013-[119]<br>75 (3)   | <b>Gene expression,</b><br><b>Mutations:</b> 10<br><b>Tumor subtypes:</b> Verhaak                             | Cox regression analysis (survival and association), Fisher exact test (imaging and genomics association)  | +VASARI features (necrosis, contrast enhancement, edema) and tumor size were found to be predictive of overall survival (see also [114])<br>+Proneural tumors were correlated to low contrast enhancement levels<br>+Mesenchymal tumors to lower degrees of nonenhanced tumors  |
| 2013-[120]<br>50 (2)   | <b>Gene expression,</b><br><b>Tumor subtypes:</b> Verhaak and Philips   | Kaplan-Meier and Cox regression (survival)  | +Increased rCBV associated to poor survival (see also [117])<br>+Survival analysis using Verhaak molecular subclassification and rCBV found to enhance patient survival models  |
| 2012-[123]<br>18(1)  | <b>Total genes:</b> 18407<br><b>Angiogenesis-associated genes:</b> 92   | Pearson correlation, hierarchical clustering (genecluster 3.0, TreeView)  | + CBV hemodynamic and PS physiologic features showed consistency in correlating positively with 7 and 5 proangiogenic genes, respectively.<br>+ Inverse correlation for CBV (3) and PS (3) with antiangiogenic genes.<br>- The study is limited by the sample size.   |
| 2012-[124]<br>78 <sup>T</sup> / 64 <sup>V</sup> (2) <sup>b</sup> | <b>Total genes:</b> 13628<br><b>micro RNAs:</b> 555<br><b>Methylation:</b> MGMT                               | Kaplan-Meir and Cox regression (survival), Excel 365, JMO Pro 10, R <sup>2</sup> statistical packages (correlation), CMS (significance probing), IPA (pathway), CMAP (functional connections) | +A 3-point GBM classification schema based on tumor Volume, patient Age, and KPS (VAK) and two classes were defined, namely VAK-A (good prognosis: 0-1 points) and VAK-B (poor prognosis: 2-3 points)<br>+VAK-A and VAK-B showed significant median survival differences<br>+ Both classes were strongly associated with a molecular gene signature   |
| 2012-[125]<br>78 (2)   | As above<br>(Affymetrix level 1 mRNA and Agilent level 2 microRNA)  | As above + miRWalk<br>(micro RNA prediction/ validation)  | +High vs low FLAIR volumes of peritumoral edema and invasion was shown to predict GBM subtypes and identify genomic components that are associated with cellular migration and invasion<br>+Above median POSTN (top upregulated gene) was associated with poor survival while high POSTN linked with low miR-219 (top downregulated microRNA) expression were associated with mesenchymal subtype |

<sup>a</sup>A distinct histopathology data set amounting 368 patients was employed as a validation set for the MRI findings that related to cell death.

<sup>b</sup>GBM patients for the validation set were further obtained from the Rembrandt: Repository for Molecular Brain Neoplasia Data dataset. 78<sup>T</sup>: 78 training patients, 64<sup>V</sup>: 64 validation patients.

IPA = Ingenuity Pathway Analysis; Cmap = connectivity map; CMS: Comparative Marker Selection; Gene Set Enrichment Analysis (GSEA); EP: Ependymal Involvement, DWMT: Deep White Matter Tract; CN: Copy Number; EGFR: Endothelial Growth Factor Receptor; PTEN: Phosphatase and Tensin Homolog; TP53: Tumor Protein p53; PDGFRA: Platelet-derived Growth Factor Receptor, Alpha Polypeptide; NER: Nonenhancing Region; rCBV : Relative Cerebral Blood Volume; EGFR: Epidermal Growth Factor Receptor;

VASARI: Visually AcceSable Rembrandt; CT: Computed Tomography; PCT: Perfusion CT; PS: Permeability Surface Area Product; VAK: Volume, patient Age, and KPS; KPS: Karnofsky Performance Status; FLAIR: Fluid Attenuated Inversion Recovery;

3D Slicer: <https://www.slicer.org/>; ePAD: <https://epad.stanford.edu/>; ClearCanvas: <https://clearcanvas.github.io/>; NordicICE: <http://www.nordicneurolab.com/products/nordicICE/>; ITK-Snap: <http://www.itksnap.org/>.

class, with MYC oncogene being the top activation regulator, as in [114]. Based on the previous findings linking MRI-FLAIR to cellular invasion in GBM, the objective in [125] was to further investigate genomic correlates of cellular invasion and molecular subtypes of GBM towards constructing a new screening tool. For that purpose, patients were further sub-classified into high, medium, and low volumes of peritumoral edema/invasion, respectively. High and low groups were selected for analysis. Key findings reported that the above median expression of the top

upregulated periostin (POSTN) gene was significantly associated with low survival and high disease progression. At the same time, high POSTN expression, when linked with low miR-219 expression, being the top downregulated microRNA, was found to correlate with mesenchymal GBM subtype.

Toward this direction, correlating radiomics phenotypes and radiogenomics signatures to GBM subtypes, is a critical research objective undertaken by TCIA research groups and radiogenomics studies in general. Verhaak classification [121]

**TABLE V**  
SELECTED NON-TCIA RADIOMICS STUDIES INVESTIGATING IMAGE-BASED CANCER PHENOTYPES

TABLE V. SELECTED NON-TCIA RADIOMICS STUDIES INVESTIGATING IMAGE-BASED CANCER PHENOTYPES

| YEAR         | DISEASE | IMAGING DATA                     | PATIENTS   | SEGMENTATION                     | DESCRIPTION   |
|--------------|---------|----------------------------------|------------|----------------------------------|---|
| 2013 - [126] | GBM     | T2/ FLAIR MRI                    | 46         | Functional Neuro Images analysis | Discriminate between mesenchymal (MES) and non-MES GBM  |
| 2016 - [127] | GBM     | Multi-modal MRI                  | 105 (29)   | GLISTR algorithm                 | Employ machine learning to perform survival analysis and discriminate between 4 GBM molecular subtypes        |
| 2016 - [128] | GBM     | MRI                              | 256 (144)  | Manual                           | Investigate GBM subtype classification and survival association based on imaging features                     |
| 2016 - [129] | NSCLC   | Chest CT                         | 79         | Semi-automated                   | Investigate prognosis assessment of stage I NSCLC after surgery   |
| 2016 - [130] | NSCLC   | PET                              | 26/ (166)a | Osirix software (manual)         | Investigate PET quantitative features association to epithelial-mesenchymal transition (EMT)                  |
| 2016 - [131] | GBM     | T1, T1c, T2, FLAIR MRI, DWI-MRI  | 120        | 3D Slicer (semi-automated)       | Investigate preoperative MRI predictive power of high grade glioma (III and IV) IDH mutation vs IDH wild-type |
| 2016 - [132] | GBM     | Multi-modal MRI                  | 37         | Vinci (semi-automated)           | Investigate discriminative power of multimodal MRI between grade II/ III and grade IV gliomas                 |
| 2017 - [133] | GBM     | DWI-MRI                          | 21         | Manual                           | Investigate DWI features correlation to GBM molecular patterns  |
| 2017 - [134] | GBM     | T1, FLAIR MRI, DSC-MRI           | 142        | Manual                           | Investigate preoperative MRI predictive power of GBM EGFRvIII mutation  |
| 2017 - [135] | GBM     | T1, T1c, T2, FLAIR MRI, DWI-MRI  | 258        | Manual                           | Examine diffusion MRI properties in predicting survival in recurrent GBM undergoing anti-VEGF treatment       |
| 2017 - [136] | NSCLC   | CT                               | 186        | ePAD (semi-automated)            | Investigate quantitative imaging to predict molecular properties (EGFR and KRAS mutations)                    |
| 2017 - [137] | LGG     | T2, FLAIR MRI                    | 125 (82)   | N/A                              | Investigate preoperative MRI predictive power of LGG IDH mutant, 1p/19q-non-codeleted molecular subtype       |
| 2018 - [138] | GBM     | T1/T2, FLAIR MRI, DTI-/ DSC- MRI | 129        | GLISTR algorithm                 | Investigate multi-modal MRI to discover a quantitative imaging signature that predicts GBM EGFRvIII mutation  |
| 2018 - [139] | LGG     | MRI                              | 25         | 3D Slicer (semi-automated)       | Investigate preoperative MRI predictive power of LGG IDH mutation vs IDH wild-type                            |
| 2018 - [140] | GBM     | T1W, T2W, FLAIR MRI              | 115        | Manual                           | Investigate tumor hypoxia characterization by radiomic features for predicting overall survival               |

GBM: Glioblastoma; LGG: Lower-Grade Glioma; NSCLC: Non-small Cell Lung Cancer; FLAIR: Fluid Attenuated Inversion Recovery; MRI: Magnetic Resonance Imaging; CT: Computed Tomography; PET: Positron Emission Tomography; DWI-MRI: Diffusion Weighted Imaging MRI, DSC-MRI: Dynamic Susceptibility Contrast MRI.

refers to GBM subclassification into classic, mesenchymal, proneural, and neural subtypes, while Phillips [122] to high-grade glioma subclassification into proneural, proliferative, and mesenchymal, based on similarity to defined genomic expression signature. In [120], relative cerebral blood volume of both the contrast-enhanced region ( $rCBV_{mean}$  and  $rCBV_{max}$ ) and the non-enhancing region ( $rCBV_{ner}$ ), showed no statistical difference between  $rCBV_{max}$ ,  $rCBV_{mean}$ , and  $rCBV_{ner}$  and the Verhaak and Phillips classification categories. On the other hand, minimum intensity edema feature was associated with mesenchymal subtype in [116], demonstrating that classic tumors have lower edema intensity than mesenchymal ones. Intensity and edge sharpness edema features as well as one necrosis feature were further found to correlate with classic tumors. In addition, authors reported on the correlation between imaging features and molecular tumour subtypes in [119]. More specifically, proneural tumors incurred low contrast-enhancement levels, while mesenchymal ones lower degrees on non-enhanced tumor, compared to other subtypes.

The authors in [124] developed a novel classifier based on tumor volume, patient age, and Karnofsky performance status (KPS) status scale termed VAK. The objective was to derive a non-invasive prognostic tool that can be exploited for patient cohort selection in clinical trials as well as a tool for genomics-based personalised treatment of GBM patients. Using a 3-point

scoring system, two classes were further defined, namely VAK-A (good prognosis) and VAK-B (poor prognosis). Experiments showed significant median survival differences between the two classes. Using an independent validation set, both classes were found to be strongly associated with a molecular gene signature including 25 genes and miRNAs, predicting survival.

### C. Non-TCIA Cancer Radiogenomics Studies

The growing research community interest in emerging radiogenomic approaches for deriving image-based cancer phenotypes is further depicted in Table V. The objective here is not to perform an exhaustive review, but rather highlight selected non-TCIA based studies by different groups that use different datasets and also investigate different cancer subtypes. Table V summarizes such approaches, namely for non-small cell lung cancer (NSCLC) [129], [130], [136], LGG [139], and GBM [126], [132], [133], [140], using different radiomic features stemming from multimodal MRI, PET, and CT image modalities.

In [129], radiogenomics for prognosis assessment of stage I NSCLC for patients undergoing surgery resulted in improved predictive power than both radiomics and genomics based biomarkers, alone. Similarly, prognostic power of a radiogenomic signature emanating from normalized fluorine 18 ( $^{18}\text{F}$ ) fluoro-2-deoxyglucose (FDG) PET images standardized

uptake value index ( $SUV_{\text{index}}$ ) and messenger RNA ( $mRNA$ ) was depicted in [130]. The signature was linked to epithelial-mesenchymal transition (EMT) molecular phenotype, increasingly associated with bad prognosis, metastasis, and chemoresistance in NSCLC, but also in other cancer types. Hand-crafted CT-based radiomic features towards predicting molecular status of NSCLC, and more specifically epidermal growth factor receptor (EGFR) and Kirsten rat sarcoma viral oncogene homolog (KRAS), EGFR's downstream, was undertaken in [136]. While predicting KRAS mutations was not feasible, models for reliably predicting EGFR wild type status and EGFR mutations were successfully derived.

In terms of GBM, quantitative MRI-based features were used for predicting MES vs non-MES [126] and grade II/III vs grade IV GBM [132], as well as correlation to molecular patterns [133], [127] and overall survival [140], [127], [128]. Interestingly, GBM subtype classification and overall survival in [128] was based on 3 imaging phenotypes derived from a pool of 388 quantitative features. Moreover, *in vivo* imaging towards identifying GBM EGFRVIII mutation was demonstrated in [134], [138]. On a different note, in [135], a post-analysis of 5 individual clinical trials resulted that diffusion MRI measurements, and more specifically baseline apparent diffusion coefficient (ADC) histogram analysis over a certain threshold, is likely to serve as overall survival predictive biomarker in recurring GBM patients that undergo anti-VEGF treatment [135]. Using preoperative MRI derived radiomic features for discriminating between IDH mutation vs IDH wild-type in LGG and high grade gliomas is yet another proof of the importance of non-invasive characterization of IDH mutation status for predicting treatment response [131], [137], [139].

#### IV. CASE STUDY II: RADIOMICS FOR MILD COGNITIVE IMPAIRMENT AND ALZHEIMER'S DISEASE

Alzheimer's disease (AD), the most common form of dementia, is a progressive age-related neurodegenerative disease which affects cognitive function and independence. It mainly affects elderly people over 65 years of age and according to Alzheimer's association, there are 47 million AD patients worldwide and by 2030 this number will climb to 76 million. Current AD research efforts focus in Mild Cognitive Impairment (MCI), a transitional period between Normal Controls (NC) and clinical AD patients. Eventually, approximately ~15% of MCI subjects will progress to AD [141]. Predicting MCI to AD conversion is a decisive factor for the earlier administration of preventive pharmaceutical interventions towards delaying the disease progression.

According to the National Institute of Neurological Disorders and Stroke-Alzheimer Disease and Related Disorders group [142], the diagnosis of AD should not rely only on clinical and psychometric assessment such as the Mini Mental State examination (MMSE) [143] and the Clinical Dementia Rating (CDR) [144]. The clinical assessment should include at least one supportive feature, such as the: (i) Medial Temporal Lobe (MTL) atrophy as seen in structural MRI, (ii) metabolic brain alterations depicted in PET, (iii) positivity on amyloid imaging available in PET, and (iv) abnormal amyloid depositions markers (tau and/or  $A\beta$ ) in cerebrospinal fluid (CSF).

Most of the studies in the assessment of AD acquire their data from the Alzheimer's Disease Neuroimaging Initiative (ADNI) database (see <http://adni.loni.usc.edu/>). ADNI was launched in 2003 as a public-private partnership, led by Principal Investigator M. W. Weiner. The primary goal of ADNI has been to test whether serial MRI, PET, other biological markers, and clinical neuropsychological assessment can be combined to measure the progression of MCI and early AD. Recognizing the value of genetic factors in AD, ADNI established the ADNI Genetics Core in 2009, underpinning combined genetics, imaging and clinical data investigation (see Fig. 1). A comprehensive review of ADNI genetic studies for quantitative MCI and AD appears in [145]. Furthermore, the Enhancing NeuroImaging Genetics through Meta-Analysis (ENIGMA) Consortium is a collaborative network of researchers working together on a range of largescale studies that integrate data from 70 institutions worldwide [146]. ENIGMA initiated in 2009 to unite researchers in imaging genomics for a better understanding on brain imaging and genetic data findings for neuroimaging phenotypes.

Genetic data have been essential in understanding the complex pathophysiology of AD. According to [147] the presence of mutations in amyloid precursor protein (APP), presenilin 1 (*PSEN1*) or presenilin 2 (*PSEN2*) can determine the early development of the disease. Furthermore, apolipoprotein E (APOE) is included in the well-established genes for AD. The APOE gene is found in human body as three polymorphic alleles:  $\epsilon 2$ ,  $\epsilon 3$  and  $\epsilon 4$  with a worldwide frequency of 8.4%, 77.9% and 13.7%, respectively. However, in an AD patient the  $\epsilon 4$  allele could increase up to ~40% [148]. Today, APOE gene represents the strongest major genetic risk for both early-onset AD (EOAD) (<65 years) and late-onset AD (LOAD) ( $\geq 65$  years), the latter representing the majority of cases, with  $\epsilon 4$  allele being the most descriptive factor [149].

Research relying on genome wide association studies (GWAS) and whole exome and whole genome sequencing data, have identified a significant number of genes that are correlated to AD. GWAS investigate single nucleotide polymorphisms (SNPs) throughout the genome to identify genetic variants of a disease which might lead to a more precise therapy. In [150], nine additional genes /loci have been identified for LOAD, namely CR1, BIN1, CLU, PICALM, MS4A4/MS4A6E, CD2AP, CD33, EPHA1 and ABCA7. A comprehensive overview of GWAS in AD appears in [151]. Furthermore, quantitative MCI phenotypes for genetic or genome-wide association studies using data from the ADNI database (published 2009–2012) are summarized in [152].

Typically, AD studies investigate imaging biomarkers, with longitudinal structural MRI data studies being the most frequent. For a review on quantitative MRI brain studies in MCI and AD, the reader is referred to [153]. However, the combination of several AD biomarkers, such as MRI scans, PiB scans, and measurements of CSF  $A\beta$  and tau or APOE allele status, significantly add predictive value to the clinical diagnosis and the evaluation of the treatment efficacy. Towards this direction, a brief overview of emerging radiogenomics methods for the assessment of AD is provided next, and tabulated in Table VI.

In [154], 742 ADNI participants were examined to map the 3D profile of the MTL volume differences. It was found that

**TABLE VI**  
ADNI-BASED RADIOMINOMICS STUDIES IN MILD COGNITIVE IMPAIRMENT AND ALZHEIMERS DISEASE

| STUDY                   | GENETIC & IMAGING DATA                                      | BIOSTATISTICAL METHODS  | DESCRIPTION   |
|-------------------------|---|---|---|
| 2010-[154]              | GWAS, sMRI  | Regression analysis, Permutation test   | SNP (rs10845840) located in GRIN2B gene, was significantly associated with the atrophy of both temporal lobes   |
| 2012-[155]              | GWAS, sMRI  | Fixed-effects, Random-effects, Haplotype analysis                                   | Intergenic variant rs7294919 associated with hippocampal volume, an HMGA2 locus rs10784502 associated with intracranial volume, and a suggestive association with total brain volume at rs10494373 within DDR2  |
| 2017-[156]              | GWAS, sMRI  | Regression coefficients, Mixed-effects models, Quantile-Quantile plots              | Four novel genome wide loci (rs11979341, rs7020341, rs2268894 and rs2289881) were associated with hippocampal volume  |
| 2016-[157]              | GWAS, sMRI  | Pearson correlation, Logistic regression, sRRR regression, <i>t-test</i>            | Left entorhinal cortex average thickness, was associated with APOE variants, and SNPs such as re59776273, rs113814152, rs79079416 and rs147030865 are suggested for further analysis Left hippocampal volume was associated with APOE variant and rs293169 SNP  |
| 2016-[158]              | APOE, Cognitive evaluation, sMRI, FDG PET, AV45-PET         | ANOVA, Chi-square test, <i>t-test</i>   | The combination of imaging, genetics and/or cognitive biomarkers better predicts MCI to AD conversion phenotype. This combination provided a 87% accuracy in the prediction of the disease compared to 76% of glucose PET as a single biomarker   |
| 2014-[159]              | Plasma proteins and sMRI                                    | Parallel independent component analysis, Pearson correlation coefficients           | This combination can provide a better prognosis and prediction of the disease. Specifically, VBM and TBM where combined with the changes in BMP6, Eselectin, MMP10 and NrCAM. In the classification of the disease a 93% sensitivity and 92% specificity was achieved. In the prediction from MCI to AD a 94% accuracy was reached  |
| 2016-[160]              | Cognitive evaluation, sMRI, APOE and TOMM40, CSF, plasma    | Receiver operating characteristic analysis  | The combination of specific plasma markers and CSF only provided 80% accuracy, 88% sensitivity and 70% specificity in predicting progression from MCI to AD   |
| 2012-[161] <sup>a</sup> | APOE, Cognitive evaluation, PET, FDG PET, sMRI, CSF         | Linear mixed effect models, Concordance correlation coefficient                     | Each biomarker follows a sigmoid shaped trajectory and is affected by interactions with age and APOE status   |
| 2016-[162]              | GWAS, sMRI, FDG-PET   | Linear regression analysis, <i>t-test/ Chi-square tests with two-sided P-values</i> | Gray matter density: No genetic influence in NC. In MCI subjects the SLC24A4/RIN3 rs10498633 and ZCWPW1 rs1476679 genes showed significant effects. Furthermore, ABCA7 rs3752246, EPHA1 rs11771145, and INPP5Dr35349669 genes were associated for AD patients. Brain metabolism: Significant associations were only seen in NC groups for SLC24A4/RIN3rs10498533, NME8 rs2718058, and CD2AP rs9349407 genes |
| 2012-[163]              | APOE, sMRI  | Logistic regression analysis, Independent-sample <i>t-test</i>                      | In APOE ε4 carriers, the V and A alleles (I405V and C-629A) of the cholesteryl ester transfer protein gene were associated with greater baseline cortical thickness and less 12-month atrophy in the MTL  |
| 2014-[164] <sup>b</sup> | Neuropsychological evaluation, APOE, β-amyloid (Ab) imaging | Linear regression analysis, Wilcoxon rank sum tests                                 | There is a strong correlation between Aβ and APOE ε4 in cognitive decline. Greater cognitive decline was present in high Aβ/APOE ε4+ participants compared to all other groups (low Aβ/APOE ε4-, low Aβ/APOE ε4+, and high Aβ/APOE ε4-)   |
| 2018-[165] <sup>c</sup> | Neuropsychological evaluation, APOE, β-amyloid (Ab) imaging | ANOVA   | Memory decline in β-amyloid-positive adults may accelerate with older age and that this increase in acceleration may be associated with the APOE ε4 allele  |
| 2017-[166]              | APOE, sMRI, FDG-PET, CSF                                    | Linear models or Logistic regression analysis                                       | MTL atrophy was less severe in subjects who had a negative β-amyloid. This was correlated with the patient's disproportionately low APOE ε4 and disproportionately high APOE ε2 carrier prevalence  |
| 2018-[167]              | APOE, sMRI, β-amyloid (Ab) imaging                          | MCMC Bayesian & GB convergence analyses   | APOE ε4 carriers had increased longitudinal accumulation of amyloid-β pathology and more atrophy in the area of MTL   |
| 2018-[168]              | APOE, β-amyloid (Ab) imaging                                | Polygenic risk scores   | APOE ε4 linked to greater memory decline and hippocampal atrophy in Aβ+ subjects  |
| 2011-[169]              | APOE, FDG-PET   | ANOVA and post-hoc two-sample <i>t-test</i>   | Longitudinal FDG-PET is associated with concurrent cognitive decline. AD subjects had higher frequency of the APOE ε4 allele gene compared to MCI and NC subjects   |
| 2014-[170]              | APOE, FDG-PET   | Linear regression, Wald tests, <i>t-test</i>  | APOE ε4 carriers had significant declines in FDG ratio  |
| 2009-[171]              | APOE, FDG-PET   | <i>t-test</i> , Linear regression analysis  | Lower CMRgl correlated with APOE ε4 allele where AD and amnestic MCI groups had higher proportion of subjects with one or two copies of the APOE ε4 allele  |
| 2012-[172]              | APOE, FDG PET- MRI  | Univariate analyses   | High APOE ε4 gene subjects were associated with lower CMRgl and lower GM volume   |
| 2011-[175]              | GWAS, sMRI, DTI   | Correlation analysis  | A potentially significant association observed for the rs2456930 polymorphism reported as a significant GWAS finding in AD. RORA, NARG2, and ADAM10 influence GM thickness and WM-FA values   |
| 2017-[176]              | APOE, sMRI (DTI and NODDY)                                  | Fisher's exact test, <i>t-test</i> , Wilcoxon rank sum test                         | Subjects with the APOE ε4 gene had more widespread WM disturbance whereas in non ε4 allele carriers the disruption was more focal   |

<sup>a</sup>Database(s): ADRC: Mayo Alzheimer's Disease research center; MCSA: Mayo Clinic study of aging; ADNI.

<sup>b</sup>Database(s): AIBL: Australian Imaging, Biomarkers and Lifestyle; HABS: Harvard Aging Brain Study; ADNI.

<sup>c</sup>Database(s): AIBL.

ADNI: Alzheimer's Disease Neuroimaging Initiative; MCI: Mild Cognitive Impairment; AD: Alzheimer's disease; sMRI: structural MRI; VBM: Voxel Based Morphometry; TBM: Tensor Based Imaging; CSF: Cerebrospinal fluid; FDG-PET: Fluorodeoxy glucose- Positron Emission Tomography; AV45-PET (florbetapir); rs-fcMRI: resting state functional connectivity MRI; TOMM40: Translocase of Outer Mitochondrial Membrane 40 homolog; NODDI: Neurite Orientation Dispersion and Density Imaging; GWAS: Genome-wide Association Studies; ANOVA: Analysis of Variance; MCMC: Markov Chain Monte Carlo; GB: Gelman-Rubin convergence; sRRR: Bonferroni correction Row-sparse reduced-rank regression ;

rs10845840 SNP located in GRIN2B gene, was significantly associated with greater atrophy of the temporal lobe bilaterally. In addition, ENIGMA's first project [155] was a GWAS study trying to identify the genome associated with hippocampal volume. Hippocampal formation is the most frequently used biomarker for the assessment of AD as it is the structure responsible for learning and memory. It was found that, intergenic variant rs7294919 was associated with hippocampal volume and rs10784502 with intracranial volume. Similarly, GWAS on 33,536 individuals (the largest study up to date) from the ENIGMA database was performed in [156]. They discovered 4 novel loci associated with hippocampal volume, three of them lying within genes (ASTN2, DPP4, MAST4) while the fourth being found 200 kb upstream of the sonic hedgehog (SHH). Hippocampal subfield analysis was also performed and it was shown that a locus within the MSRB3 gene could affect the dentate gyrus, subiculum, CA1 and fissure.

In [157], a Bayesian method to identify indirect genetic associations between AD and NC using image phenotypes was used. Associations between imaging and disease phenotype were captured simultaneously with the correlation from genetic variants and image features in a probabilistic model. In the model, brain regions not associated with AD were not included even if they were strongly modulated by genetics. In addition to the APOE variants, the study concluded that more SNPs are suggested for further investigation (see Table VI).

In [158]–[160], the authors showed that the combination of imaging, genetics and neuropsychological tests could provide better accuracy in the prediction to AD conversion compared to single modality classifiers. Combined CSF, MRI, PET and genomics were used in [161] to investigate the shapes of trajectories of AD biomarkers as a function of MMSE, demonstrating that a sigmoidal shape over time is followed. Brain metabolism and gray matter (GM) density combined with GWAS to identify the genetic influences on NC, MCI and AD subjects was investigated in [162]. Key findings linked most genes' effects with the stage of the disease (see also Table VI).

APOEs is the strongest genetic predictor of AD. Toward this direction, the study in [163] revealed that specific alleles in APOE  $\varepsilon 4$  carriers, correlated with a more severe cortical thickness and MTL atrophy. Moreover, APOE  $\varepsilon 4$  carriers who had a high  $\beta$ - amyloid ( $A\beta$ ) PET imaging, were more affected by cognitive decline as depicted in [164], [165]. Their results were correlated with [166] where subjects with negative  $\beta$ - amyloid peptide scan had less temporoparietal hypometabolism, less severe MTL atrophy, and low APOE  $\varepsilon 4$  gene. In a longitudinal study [167], the authors followed a whole brain approach using MRI and PET and showed that  $\varepsilon 4$  allele carriers had faster rates of cortical loss, especially in the area of MTL, and increased longitudinal accumulation of amyloid- $\beta$  pathology on their cortex. Importantly, the study suggested that APOE gene influences on AD could be detected in middle age. Similarly, in [168], APOE  $\varepsilon 4$  was strongly related to baseline  $A\beta$  and to greater memory decline and hippocampal atrophy in  $A\beta+$  subjects.

Moreover, in [169], it was shown that lower baseline FDG PET can predict subsequent cognitive decline while APOE  $\varepsilon 4$  allele was more frequent in AD compared to MCI and NC

subjects. A reduction in glucose metabolism was also seen in APOE  $\varepsilon 4$  allele carriers in AD-signature ROIs in [170]. The author in [171], compared baseline regional cerebral metabolic rate for glucose (CMRgI) using FDG PET in mildly affected AD subjects and 142 amnestic MCI subjects to those from NC. As expected, compared to NC, AD and amnestic MCI subjects had significantly lower CMRgI bilaterally (in posterior cingulate, precuneus, parietotemporal and frontal cortex) which was correlated with MMSE scores and APOE  $\varepsilon 4$  allele. The results were correlated with the study in [172].

Diffusion tensor imaging (DTI) is a MRI technique that allows the assessment of the microstructural integrity of White Matter (WM) based on fractional anisotropy (FA) and mean diffusivity (MD). It was found that the microstructural integrity of WM tends to follow an anterior to posterior path with MCI and AD subjects having more damage in posterior regions [173]. Furthermore, the authors in [174] used DTI to measure FA and revealed a reduction in cingulum fibers in the parahippocampal and posterior cingulate regions of MCI and AD subjects. In [175], structural MRI and DTI was used to assess the cortical GM thickness and fractional anisotropy. Their analysis indicated that RORA, NARG2, and ADAM10 influences GM thickness and WM-FA values. In [176], DTI-MRI and neurite orientation dispersion and density imaging (NODDI) with tract-based spatial statistics was used to investigate APOE  $\varepsilon 4$  modulation of WM damage in subjects with young onset AD. Interestingly, different WM changes in pre-symptomatic stages of AD were detected.

## V. DISCUSSION AND CONCLUDING REMARKS

Building on multi-institutional collaboration and driven by open research data initiatives, the emerging area of radiogenomics holds great promise for precision medicine. Recent retrospective studies in cancer and Alzheimer's disease reviewed in this study, show that new radiogenomics biomarkers can elucidate non-invasive stratification of patients, contributing towards enhanced prognosis, diagnosis, and treatment. Yet, precision medicine using radiogenomics in daily care remains a challenge. Beyond publications, only a portion of new biomarkers are patented, and an even smaller percentage adopted in standard clinical practice [177].

In that context, there is a strong need to collect, annotate, and classify large datasets for many diseases that go beyond CIP and ADNI. Ideally, some of the methods that were discussed in this paper will also find applications in other diseases as well.

At the same time, there is clearly a tradeoff between strong classification performance achieved by complex neural networks versus somewhat lower performance achieved by more conventional approaches. To avoid overfitting, we recommend the adoption of simpler and better-understood classifiers that may sacrifice some (but not a significant amount) of the performance.

More generally, there is a need for explainable methods. As mentioned in the introduction, clinically relevant feature extraction is a primary message of this paper. Future research should

also favor image analysis solutions that can be easily visualized (e.g., see segmentation regions in Fig. 2). In terms of deep neural nets, it is important to visualize the outputs of each one of the combined convolutional and pool layers (see Table I) in a comprehensible manner. Additionally, advancing hybrid methods that combine information from different imaging modalities and biomarkers are essential.

Despite the challenges, initiatives such as the CIP and ADNI, reinforced by invested policy makers in both the EU and the USA, create a momentum that allows optimism. Moreover, oncology and central nervous system clinical application areas, rank 1st and 3rd in the Global precision medicine market, with a projected size of \$57.09 billion (CAGR: 10.44%) and \$14.40 billion (CAGR: 14.40%) by 2026, respectively [4]. At the same time, big data technologies, and especially deep learning, support knowledge discovery from the wealth of big healthcare data available today. The latter, is expected to drive advances in the near future, towards establishing radiogenomics as a key precision medicine discipline.

## REFERENCES

- [1] K. Hudson *et al.*, “The precision medicine initiative cohort program—building a research foundation for 21st century medicine,” Precision Medicine Initiative, NIH, Bethesda, MD, USA, 2015.
- [2] Personalised Medicine Coalition, [Online]. Available: <http://www.personalizedmedicinecoalition.org/>, Accessed on: Sep. 2018.
- [3] European Alliance on Personalized Medicine, [Online]. Available: <https://www.euapm.eu/>, Accessed on: Sep. 2018.
- [4] “Global precision medicine market—analysis and forecast (2017–2026),” BIS Res., Fremont, CA, USA, 2017.
- [5] H. J. Aerts, “The potential of radiomic-based phenotyping in precision medicine: a review,” *JAMA Oncol.*, vol. 2, no. 12, pp. 1636–1642, 2016.
- [6] T. E. Yankelev, R. G. Abramson, and C. C. Quarles, “Quantitative multimodality imaging in cancer research and therapy,” *Nature Rev. Clin. Oncol.*, vol. 11, no. 11, pp. 670–80, 2014.
- [7] V. Kumar *et al.*, “Radiomics: The process and the challenges,” *Magn. Resonan. Imag.*, vol. 30, no. 9, pp. 1234–1248, 2012.
- [8] R. J. Gillies, P. E. Kinahan, and H. Hricak, “Radiomics: Images are more than pictures, they are data,” *Radiology*, vol. 278, no. 2, pp. 563–577, 2015.
- [9] P. Lambin *et al.*, “Radiomics: The bridge between medical imaging and personalized medicine,” *Nature Rev. Clin. Oncol.*, vol. 14, no. 12, pp. 749–762, 2016.
- [10] C. C. Jaffe, “Imaging and genomics: Is there a synergy?” *Radiology*, vol. 264, no. 2, pp. 329–331, 2012.
- [11] G. Lee *et al.*, “Radiomics and imaging genomics in precision medicine,” *Precis. Future Med.*, vol. 1, no. 1, pp. 10–31, 2017.
- [12] A. M. Rutman and D. K. Michael, “Radiogenomics: Creating a link between molecular diagnostics and diagnostic imaging,” *Eur. J. Radiol.*, vol. 70, no. 2, pp. 232–241, 2009.
- [13] K. Pinker *et al.*, “Precision medicine and radiogenomics in breast cancer: New approaches toward diagnosis and treatment,” *Radiology*, vol. 287, no. 3, pp. 732–747, 2018.
- [14] S. G. Megason and S. E. Fraser, “Imaging in systems biology,” *Cell*, vol. 130, no. 5, pp. 784–795, 2007.
- [15] Z. Liu and P. J. Keller, “Emerging imaging and genomic tools for developmental systems biology,” *Develop. Cell*, vol. 36, no. 6, pp. 597–610, 2016.
- [16] Y. LeCun, Y. Bengio, and G. Hinton, “Deep learning,” *Nature*, vol. 521, no. 7553, pp. 436–444, 2015.
- [17] J. Andreu-Perez, C. C. Y. Poon, R. D. Merrifield, S. T. C. Wong, and G. Z. Yang, “Big data for health,” *IEEE J. Biomed. Health Inform.*, vol. 19, no. 4, pp. 1193–1208, Jul. 2015.
- [18] M. Viceconti, P. Hunter, and R. Hose, “Big data, big knowledge: Big data for personalized healthcare,” *IEEE J. Biomed. Health Inform.*, vol. 19, no. 4, pp. 1209–1215, Jul. 2015.
- [19] J. Luo, M. Wu, D. Gopukumar, and Y. Zhao, “Big data application in biomedical research and health care: A literature review,” *Biomed. Inform. Insights*, vol. 8, p. BII-S31559, 2016.
- [20] J. Sun and C. K. Reddy, “Big data analytics for healthcare,” in *Proc. Tut. Presentation, SIAM Int. Conf. Data Mining*, ACM, Aug. 2013, pp. 1525–1525.
- [21] E. A. Mohammed, B. H. Far, and C. Naugler, “Applications of the mapreduce programming framework to clinical big data analysis: Current landscape and future trends,” *BioData Mining*, vol. 7, no. 22, pp. 1–23, 2014.
- [22] H. Hu, Y. Wen, T. S. Chua, and X. Li, “Toward scalable systems for big data analytics: A technology tutorial,” *IEEE Access*, vol. 2, pp. 652–687, 2014.
- [23] Dieter Haas, Big Data: Image & Video Analytics: How it could support Archiving & Indexing & Searching, IBM Deutschland GmbH, 2014.
- [24] C. S. Kruse *et al.*, “Challenges and opportunities of big data in health care: A systematic review,” *JMIR Med. Inform.*, vol. 4, no. 4, 2016.
- [25] I. El Naqa, “Perspectives on making big data analytics work for oncology,” *Methods*, vol. 111, pp. 32–44, 2016.
- [26] P. Y. Wu *et al.*, “–Omic and electronic health record big data analytics for precision medicine,” *IEEE Trans. Biomed. Eng.*, vol. 64, no. 2, pp. 263–273, Feb. 2017.
- [27] The Cancer Imaging Archive, [Online]. Available: <http://www.cancerimagingarchive.net/>, Accessed on: Sep. 2018.
- [28] K. Clark *et al.*, “The cancer imaging archive (TCIA): Maintaining and operating a public information repository,” *J. Digit. Imag.*, vol. 26, no. 6, pp. 1045–1057, 2013.
- [29] The Alzheimer’s Disease Neuroimaging Initiative (ADNI), [Online]. Available: <http://adni.loni.usc.edu/>, Accessed on: Sep. 2018.
- [30] B. M. Ellingson *et al.*, “Consensus recommendations for a standardized brain tumor imaging protocol in clinical trials,” *Neuro-Oncol.*, vol. 17, no. 9, pp. 1188–1198, 2015.
- [31] The Alzheimer’s Disease Neuroimaging Initiative, Methods and Tools, [Online]. Available: <http://adni.loni.usc.edu/methods/>, Accessed on Sep. 2018.
- [32] “Digital imaging and communications in medicine (dicom), part 15: Security and system management profiles,” DICOM Standard PS 3.15-2011, [Online]. Available: [ftp://medical.nema.org/medical/dicom/2016b/output/html/part15.html#chapter\\_E](ftp://medical.nema.org/medical/dicom/2016b/output/html/part15.html#chapter_E). Accessed on: Sep. 2018.
- [33] S. Bakas *et al.*, “Advancing the cancer genome atlas glioma MRI collections with expert segmentation labels and radiomic features,” *Sci. Data*, vol. 4, 2017, Art. no. 170117.
- [34] B. H. Menze *et al.*, “The multimodal brain tumor image segmentation benchmark (BRATS),” *IEEE Trans. Med. Imag.*, vol. 34, no. 10, pp. 1993–2024, Oct. 2015.
- [35] W. Guo *et al.*, “Prediction of clinical phenotypes in invasive breast carcinomas from the integration of radiomics and genomics data,” *J. Med. Imag.*, vol. 2, no. 4, 2015, Art. no. 041007.
- [36] L. Wei *et al.*, “TCGA-assembler 2: Software pipeline for retrieval and processing of TCGA/CPTAC Data,” *Bioinformatics*, vol. 1, pp. 1615–1617, 2017.
- [37] L. Varemo *et al.*, “Enriching the gene set analysis of genome-wide data by incorporating directionality of gene expression and combining statistical hypotheses and methods,” *Nucleic Acids Res.*, vol. 41, pp. 4378–4391, 2013.
- [38] A. Krämer *et al.*, “Causal analysis approaches in ingenuity pathway analysis,” *Bioinformatics*, vol. 30, no. 4, pp. 523–530, 2013.
- [39] C. Parmar *et al.*, “Machine learning methods for quantitative radiomic biomarkers,” *Sci. Rep.*, vol. 5, 2015, Art. no. 13087.
- [40] E. L. Kaplan and P. Meier, “Nonparametric estimation from incomplete observations,” *J. Amer. Stat. Assoc.*, vol. 53, no. 282, pp. 457–481, 1958.
- [41] M. V. Rijmenam, “The body as a source of big data – infographic,” DATAFLOQ B.V, Aug. 2016.
- [42] A. S. Panayides, C. S. Pattichis, and M. S. Pattichis, “The promise of big data technologies and challenges for image and video analytics in healthcare,” in *Proc. 2016 50th Asilomar Conf. Signals, Syst. Comput., Pacific Grove*, 2016, pp. 1278–1282.
- [43] G. Quellec, G. Cazuguel, B. Cochener, and M. Lamard, “Multiple-instance learning for medical image and video analysis,” *IEEE Reviews Biomed. Eng.*, vol. 10, pp. 213–234, 2017.
- [44] A. P. James and B. V. Dasarathy, “Medical image fusion: A survey of the state of the art,” *Inform. Fusion*, vol. 19, pp. 4–19, 2014.

- [45] R. Fang, S. Pouyanfar, Y. Yang, S. C. Chen, and S. S. Iyengar, "Computational health informatics in the big data age: A survey," *ACM Comput. Surveys*, vol. 49, no. 1, 2016, Art. no. 12.
- [46] G. Varoquaux, "Cross-validation failure: Small sample sizes lead to large error bars," *NeuroImage*, Jun. 2017.
- [47] M. D. Wilkinson *et al.*, "The FAIR guiding principles for scientific data management and stewardship," *Sci. Data*, vol. 3, 2016, doi: [10.1038/sdata.2016.18](https://doi.org/10.1038/sdata.2016.18).
- [48] B. Zhao *et al.*, "Reproducibility of radiomics for deciphering tumor phenotype with imaging," *Sci. Rep.*, vol. 6, 2016, Art. no. 23428.
- [49] Integrating the Healthcare Enterprise, [Online]. Available : <https://www.ihe.net/>, Accessed on: Sep. 2018.
- [50] V. Tresp *et al.*, "Going digital: A survey on digitalization and large-scale data analytics in healthcare," *Proc. IEEE*, vol. 104, no. 11, pp. 2180–2206, Nov. 2016.
- [51] M. Chen, Y. Qian, J. Chen, K. Hwang, S. Mao, and L. Hu, "Privacy protection and intrusion avoidance for cloudlet-based medical data sharing," *IEEE Trans. Cloud Comput.*, doi: [10.1109/TCC.2016.2617382](https://doi.org/10.1109/TCC.2016.2617382).
- [52] Grand Challenges in Biomedical Image Analysis, [Online]. Available: <https://grand-challenge.org/>, Accessed on: Sep. 2018.
- [53] The Cancer Imaging Archive Competitions, [Online]. Available: <https://wiki.cancerimagingarchive.net/display/Public/Challenge+competitions>, Accessed on: Sep. 2018.
- [54] R. V. Marinescu *et al.*, "TADPOLE Challenge: Prediction of longitudinal evolution in alzheimer's disease," 2018, arxiv:1805.03909.
- [55] O. Russakovsky *et al.*, "Imagenet large scale visual recognition challenge," *Int. J. Comput. Vis.*, vol. 115, no. 3, pp. 211–252, 2015.
- [56] A. Krizhevsky, S. Ilya, and E. H. Geoffrey, "Imagenet classification with deep convolutional neural networks," *Adv. Neural Inform. Process. Syst.*, vol. 60, pp. 1097–1105, 2012.
- [57] C. Szegedy *et al.*, "Going deeper with convolutions," in *Proc. IEEE Conf. Comput. Vis. Pattern Recognit.*, 2015, pp. 1–9.
- [58] K. Simonyan and A. Zisserman, "Very deep convolutional networks for large-scale image recognition," Sep. 2014, arXiv preprint arxiv:1409.1556.
- [59] F. N. Iandola *et al.*, "SqueezeNet: Alexnet-level accuracy with 50x fewer parameters and < 0.5 MB model size," Feb. 2016, arxiv:1602.07360.
- [60] K. He, X. Zhang, S. Ren, and J. Sun, "Deep residual learning for image recognition," in *Proc. IEEE Conf. Comput. Vis. Pattern Recognit.*, 2016, pp. 770–778.
- [61] Y. Jia *et al.*, "Caffe: Convolutional architecture for fast feature embedding," in *Proc. 22nd ACM Int. Conf. Multimedia*, 2014, pp. 675–678.
- [62] PyTorch deep learning framework, [Online]. Available: <http://pytorch.org/>, Accessed on: Sep. 2018.
- [63] Keras: The Python Deep Learning Library, [Online]. Available: <https://keras.io/>, Accessed on: Sep. 2018.
- [64] F. Bastien *et al.*, "Theano: New features and speed improvements," Nov. 2012, arxiv preprint arXiv:1211.5590.
- [65] M. Abadi *et al.*, "TensorFlow: A system for large-scale machine learning," in *Proc. Oper. Syst. Des. Implement.*, 2016, vol. 16, pp. 265–283.
- [66] Microsoft Cognitive Toolkit (CNTK), An Open-source Deep Learning Toolkit, [Online]. Available: <https://docs.microsoft.com/en-us/cognitive-toolkit/>, Accessed on: Sep. 2018.
- [67] M. A. Alsmirat *et al.*, "Accelerating compute intensive medical imaging segmentation algorithms using hybrid CPU-GPU implementations," *Multimedia Tools Appl.*, vol. 76, no. 3, pp. 3537–3555, 2017.
- [68] NVIDIA DIGITS, Interactive Deep Learning GPU Training System, [Online]. Available: <https://developer.nvidia.com/digits>, Accessed on: Sep. 2018.
- [69] H. Greenspan, B. van Ginneken, and R. M. Summers, "Guest editorial deep learning in medical imaging: Overview and future promise of an exciting new technique," *IEEE Trans. Med. Imag.*, vol. 35, no. 5, pp. 1153–1159, May. 2016.
- [70] G. Litjens *et al.*, "A survey on deep learning in medical image analysis," 2017, arxiv:1702.05747.
- [71] K. Yasaka *et al.*, "Deep learning with convolutional neural network in radiology," *Jpn. J. Radiol.*, vol. 36, pp. 257–272, 2018.
- [72] H. C. Shin *et al.*, "Deep convolutional neural networks for computer-aided detection: CNN architectures, dataset characteristics and transfer learning," *IEEE Trans. Med. Imag.*, vol. 35, no. 5, pp. 1285–1298, May 2016.
- [73] N. Tajbakhsh *et al.*, "Convolutional neural networks for medical image analysis: Full training or fine tuning?," *IEEE Trans. Med. Imag.*, vol. 35, no. 5, pp. 1299–1312, May 2016.
- [74] P. P. Ypsilantis *et al.*, "Predicting response to neoadjuvant chemotherapy with pet imaging using convolutional neural networks," *PLoS one*, vol. 10, no. 9, 2015, Art. no. e0137036.
- [75] Z. Li, Y. Wang, J. Yu, Y. Guo, and W. Cao, "Deep learning based radiomics (DLR) and its usage in noninvasive IDH1 prediction for low grade glioma," *Sci. Rep.*, vol. 7, no. 1, Jul. 2017, Art. no. 5467.
- [76] J. Lao *et al.*, "A deep learning-based radiomics model for prediction of survival in glioblastoma multiforme," *Sci. Rep.*, vol. 7, no. 1, Sep. 2017, Art. no. 10353.
- [77] P. Eichinger *et al.*, "Diffusion tensor image features predict IDH genotype in newly diagnosed WHO grade II/III gliomas," *Sci. Rep.*, vol. 7, no. 1, Oct. 2017, Art. no. 13396.
- [78] P. Korfiatis, T. L. Kline, D. H. Lachance, I. F. Parney, J. C. Buckner, and B. J. Erickson, "Residual deep convolutional neural network predicts MGMT methylation status," *J. Digit. Imag.*, vol. 30, no. 5, pp. 622–628, 2017.
- [79] Z. Zhu, E. Albadawy, A. Saha, J. Zhang, M. R. Harowicz, and M. A. Mazurowski, "Deep learning for identifying radiogenomic associations in breast cancer," Nov. 2017, arXiv:1711.11097.
- [80] K. Chang *et al.*, "Residual convolutional neural network for the determination of IDH status in low-and high-grade gliomas from MR imaging," *Clin. Cancer Res.*, vol. 24, no. 5, pp. 1073–1081, 2018.
- [81] P. Korfiatis *et al.*, "Evaluation of a deep learning architecture for MR imaging prediction of ATRX in glioma patients," *Proc. SPIE*, vol. 10575, 2018, Art. no. 10575G.
- [82] K. H. Cha *et al.*, "Bladder cancer treatment response assessment in CT using radiomics with deep-learning," *Sci. Rep.*, vol. 7, no. 1, 2017, Art. no. 8738.
- [83] L. Oakden-Rayner *et al.*, "Precision radiology: Predicting longevity using feature engineering and deep learning methods in a radiomics framework," *Sci. Rep.*, vol. 7, no. 1, May 2017, Art. no. 1648.
- [84] K. Kamnitsas *et al.*, "Efficient multi-scale 3D CNN with fully connected CRF for accurate brain lesion segmentation," *Med. Image Anal.*, vol. 36, pp. 61–78, 2017.
- [85] A. Ulloa *et al.*, "An unsupervised homogenization pipeline for clustering similar patients using electronic health record data," 2017, arxiv:1801.00065.
- [86] A. Rajkomar *et al.*, "Scalable and accurate deep learning with electronic health records," *Npj Digit. Med.*, vol. 1, no. 1, 2018, Art. no. 18.
- [87] A. Aliper *et al.*, "Deep learning applications for predicting pharmacological properties of drugs and drug repurposing using transcriptomic data," *Mol. Pharmaceutics*, vol. 13, no. 7, pp. 2524–2530, 2016.
- [88] S. Min *et al.*, "Deep learning in bioinformatics," *Briefings Bioinf.*, vol. 18, no. 5, pp. 851–869, 2017.
- [89] M. Längkvist *et al.*, "A review of unsupervised feature learning and deep learning for time-series modelling," *Pattern Recogni. Letters*, vol. 42, pp. 11–24, 2014.
- [90] "Comprehensive molecular characterization of urothelial bladder carcinoma," *Nature*, vol. 507, no. 7492, pp. 315–322, 2014.
- [91] G. Ciriello *et al.*, "Comprehensive molecular portraits of invasive lobular breast cancer," *Cell*, vol. 163, no. 2, pp. 506–519, 2015.
- [92] C. W. Brennan *et al.*, "The somatic genomic landscape of glioblastoma," *Cell*, vol. 155, no. 2, pp. 462–477, 2013.
- [93] "Comprehensive, integrative genomic analysis of diffuse lower-grade gliomas," *New England J. Med.*, vol. 372, no. 26, pp. 2481–2498, 2015.
- [94] B. M. Ellington, "Radiogenomics and imaging phenotypes in glioblastoma: Novel observations and correlation with molecular characteristics," *Current Neurol. Neurosci. Rep.*, vol. 15, no. 1, pp. 506:1–12, 2015.
- [95] M. Parfenov *et al.*, "Characterization of HPV and host genome interactions in primary head and neck cancers," *Proc. Nat. Acad. Sci.*, vol. 111, no. 43, pp. 15544–15549, 2014.
- [96] "Comprehensive molecular characterization of clear cell renal cell carcinoma," *Nature*, vol. 499, no. 7456, pp. 43–49, 2013.
- [97] "Integrated genomic analyses of ovarian carcinoma," *Nature*, vol. 474, no. 7353, pp. 609–615, 2011.
- [98] TCIA Analysis Results, [Online]. Available: <https://wiki.cancerimagingarchive.net/display/DOI/TCIA+Analysis+Results>, Accessed on: Sep. 2018.
- [99] A. B. Shinagare *et al.*, "Radiogenomics of clear cell renal cell carcinoma: Preliminary findings of the cancer genome atlas–renal cell carcinoma (TCGA–RCC) imaging research group," *Abdominal Imag.*, vol. 40, no. 6, pp. 1684–1692, 2015.
- [100] E. S. Burnside *et al.*, "Using computer-extracted image phenotypes from tumors on breast magnetic resonance imaging to predict breast cancer pathologic stage," *Cancer*, vol. 122, no. 5, pp. 748–757, 2016.

- [101] Y. Zhu *et al.*, “Deciphering genomic underpinnings of quantitative MRI-based radiomic phenotypes of invasive breast carcinoma,” *Sci. Rep.*, vol. 5, 2015, Art. no. 17787.
- [102] M. Kanehisa *et al.*, “KEGG for integration and interpretation of large-scale molecular data sets,” *Nucleic Acids Res.*, vol. 40, pp. D109–114, 2012.
- [103] H. Li *et al.*, “MR imaging radiomics signatures for predicting the risk of breast cancer recurrence as given by research versions of mammaprint, oncotype DX, and PAM50 gene assays,” *Radiology*, vol. 281, no. 2, pp. 382–391, 2016.
- [104] H. Li *et al.*, “Quantitative MRI radiomics in the prediction of molecular classifications of breast cancer subtypes in the TCGA/TCIA data set,” *NPJ Breast Cancer*, vol. 2, 2016, Art. no. 16012.
- [105] Y. Zhu *et al.*, “TCGA-assembler: Open-source software for retrieving and processing TCGA data,” *Nat. Methods*, vol. 11, no. 6, pp. 599–600, 2014.
- [106] W. Chen, M. L. Giger, and U. Bick, “A fuzzy c-means (FCM)-based approach for computerized segmentation of breast lesions in dynamic contrast-enhanced MR images,” *Acad. Radiol.*, vol. 13, no. 1, pp. 63–72, 2006.
- [107] D. N. Louis *et al.*, “The 2016 world health organization classification of tumors of the central nervous system: A summary,” *Acta Neuropatholog.*, vol. 131, no. 6, pp. 803–20, Jun. 2016.
- [108] “Wiki for the VASARI feature set.” Cancer Imag. Archive, Nat. Cancer Inst., Rockville, MD, USA, [Online]. Available: <https://wiki.cancerimagingarchive.net/display/Public/VASARI+Research+Project>, Accessed on: Sep. 2018.
- [109] “Image based examples of how the VASARI feature set was utilized in round 1,” VASARI MRI Visual Feature Guide, [Online]. Available: <https://wiki.cancerimagingarchive.net/display/Public/VASARI+Research+Project>, Accessed on: Sep. 2018.
- [110] VASARI MR Feature Key, Available Online: [https://wiki.nci.nih.gov/download/attachments/14877082/VASARI\\_MR\\_featurekey4\\_508\\_compliant.pdf?version=1&modificationDate=1350523920000](https://wiki.nci.nih.gov/download/attachments/14877082/VASARI_MR_featurekey4_508_compliant.pdf?version=1&modificationDate=1350523920000), Accessed on: Sep. 2018.
- [111] N. Porz *et al.*, “Multi-modal glioblastoma segmentation: Man versus machine,” *PloS one*, vol. 9, no. 5, 2014, Art. no. e96873.
- [112] E. R. Velazquez *et al.*, “Fully automatic GBM segmentation in the TCGA-GBM dataset: Prognosis and correlation with VASARI features,” *Sci. Rep.*, vol. 5, 2015, Art. no. 16822, doi: [10.1038/srep16822](https://doi.org/10.1038/srep16822).
- [113] S. Bauer *et al.*, “A survey of MRI-based medical image analysis for brain tumor studies,” *Phys. Med. Biol.*, vol. 58, no. 13, pp. R97–129, 2013.
- [114] R. R. Colen, J. Wang, S. K. Singh, D. A. Gutman, and P. O. Zinn, “Glioblastoma: Imaging genomic mapping reveals sex-specific oncogenic associations of cell death,” *Radiology*, vol. 275, no. 1, pp. 215–227, 2014.
- [115] R. R. Colen *et al.*, “Imaging genomic mapping of an invasive MRI phenotype predicts patient outcome and metabolic dysfunction: A TCGA glioma phenotype research group project,” *BMC Med. Genomics*, vol. 7, no. 1, pp. 30:1–9, 2014.
- [116] O. Gevaert *et al.*, “Glioblastoma multiforme: Exploratory radiogenomic analysis by using quantitative image features,” *Radiology*, vol. 273, no. 1, pp. 168–174, 2014.
- [117] R. Jain *et al.*, “Outcome prediction in patients with glioblastoma by using imaging, clinical, and genomic biomarkers: Focus on the nonenhancing component of the tumor,” *Radiology*, vol. 272, no. 2, pp. 484–493, 2014.
- [118] M. Nicolasjilwan *et al.*, “Addition of MR imaging features and genetic biomarkers strengthens glioblastoma survival prediction in TCGA patients,” *J. Neuroradiol.*, vol. 42, no. 4, pp. 212–221, 2015.
- [119] D. A. Gutman *et al.*, “MR imaging predictors of molecular profile and survival: Multi-institutional study of the TCGA glioblastoma data set,” *Radiology*, vol. 267, no. 2, pp. 560–569, 2013.
- [120] R. Jain *et al.*, “Genomic mapping and survival prediction in glioblastoma: Molecular subclassification strengthened by hemodynamic imaging biomarkers,” *Radiology*, vol. 267, no. 1, pp. 212–220, 2013.
- [121] R. G. Verhaak *et al.*, “Integrated genomic analysis identifies clinically relevant subtypes of glioblastoma characterized by abnormalities in PDGFRA, IDH1, EGFR, and NF1,” *Cancer Cell*, vol. 17, no. 1, pp. 98–110, 2010.
- [122] H. S. Phillips *et al.*, “Molecular subclasses of high-grade glioma predict prognosis, delineate a pattern of disease progression, and resemble stages in neurogenesis,” *Cancer Cell*, vol. 9, no. 3, pp. 157–173, 2006.
- [123] R. Jain *et al.*, “Correlation of perfusion parameters with genes related to angiogenesis regulation in glioblastoma: A feasibility study,” *Amer. J. Neuroradiol.*, vol. 33, no. 7, pp. 1343–1348, 2012.
- [124] P. O. Zinn *et al.*, “A novel volume-age-KPS (VAK) glioblastoma classification identifies a prognostic cognate microRNA-gene signature,” *PloS one*, vol. 7, no. 8, 2012, Art. no. e41522.
- [125] P. O. Zinn *et al.*, “Radiogenomic mapping of edema/cellular invasion MRI-phenotypes in glioblastoma multiforme,” *PloS one*, vol. 6, no. 10, 2011, Art. no. e25451.
- [126] K. M. Naeini *et al.*, “Identifying the mesenchymal molecular subtype of glioblastoma using quantitative volumetric analysis of anatomic magnetic resonance images,” *Neuro-Oncol.*, vol. 15, no. 5, pp. 626–634, 2013.
- [127] L. Macyszyn *et al.*, “Imaging patterns predict patient survival and molecular subtype in glioblastoma via machine learning techniques,” *Neuro-Oncol.*, vol. 18, 3, pp. 417–425, 2015.
- [128] H. Itakura *et al.*, “Magnetic resonance image features identify glioblastoma phenotypic subtypes with distinct molecular pathway activities,” *Sci. Transl. Med.*, vol. 7, no. 303, 2015, Art. no. 303ra138.
- [129] N. Emaminejad *et al.*, “Fusion of quantitative image and genomic biomarkers to improve prognosis assessment of early stage lung cancer patients,” *IEEE Trans. Biomed. Eng.*, vol. 63, no. 5, pp. 1034–1043, May 2016.
- [130] S. Yamamoto *et al.*, “Radiogenomic analysis demonstrates associations between 18F-fluoro-2-deoxyglucose PET, prognosis, and epithelial-mesenchymal transition in non-small cell lung cancer,” *Radiology*, vol. 280, no. 1, pp. 261–270, Apr. 2016.
- [131] B. Zhang *et al.*, “Multimodal MRI features predict isocitrate dehydrogenase genotype in high-grade gliomas,” *Neuro-Oncol.*, vol. 19, pp. 109–117, 2016.
- [132] B. Wiestler *et al.*, “Multiparametric MRI-based differentiation of WHO grade II/III glioma and WHO grade IV glioblastoma,” *Sci. Rep.*, vol. 6, 2016, Art. no. 35142.
- [133] D. H. Heiland *et al.*, “Integrative diffusion-weighted imaging and radiogenomic network analysis of glioblastoma multiforme,” *Sci. Rep.*, vol. 7, 2017, Art. no. 43523.
- [134] S. Bakas *et al.*, “In vivo detection of EGFRvIII in glioblastoma via perfusion magnetic resonance imaging signature consistent with deep peritumoral infiltration: The  $\varphi$ -index,” *Clin. Cancer Res.*, vol. 23, pp. 4724–4734, 2017.
- [135] B. M. Ellingson *et al.*, “Diffusion MRI phenotypes predict overall survival benefit from anti-VEGF monotherapy in recurrent glioblastoma: Converging evidence from phase II trials,” *Clin. Cancer Res.*, vol. 23, pp. 5745–5756, 2017.
- [136] O. Gevaert *et al.*, “Predictive radiogenomics modeling of EGFR mutation status in lung cancer,” *Sci. Rep.*, vol. 7, 2017, Art. no. 41674.
- [137] S. H. Patel *et al.*, “T2-FLAIR mismatch, an imaging biomarker for IDH and 1p/19q status in lower grade gliomas: A TCGA/TCIA project,” *Clin. Cancer Res.*, vol. 23, pp. 6078–6085, 2017.
- [138] H. Akbari *et al.*, “In vivo evaluation of EGFRvIII mutation in primary glioblastoma patients via complex multiparametric MRI signature,” *Neuro-Oncol.*, vol. 20, pp. 1068–1079, 2018.
- [139] A. S. Jakola *et al.*, “Quantitative texture analysis in the prediction of IDH status in low-grade gliomas,” *Clin. Neurol. Neurosurgery*, vol. 164, pp. 114–120, Jan. 2018.
- [140] N. Beig *et al.*, “Radiogenomic analysis of hypoxia pathway is predictive of overall survival in glioblastoma,” *Sci. Rep.*, vol. 8, no. 1, 2018, Art. no. 7.
- [141] S. T. Farias *et al.*, “Progression of mild cognitive impairment to dementia in clinic- vs community-based cohorts,” *Arch. Neurol.*, vol. 66, no. 9, pp. 1151–1157, Sep. 2009.
- [142] B. Dubois *et al.*, “Research criteria for the diagnosis of Alzheimer’s disease: Revising the NINCDS-ADRDA criteria,” *Lancet Neurol.*, vol. 6, no. 8, pp. 734–746, Aug. 2007.
- [143] M. F. Folstein, S. E. Folstein, and P. R. McHugh, “‘Mini-mental state’: a practical method for grading the cognitive state of patients for the clinician,” *J. Psychiatr. Res.*, vol. 12, no. 3, pp. 189–198, Nov. 1975.
- [144] J. C. Morris, “The clinical dementia rating (CDR): Current version and scoring rules,” *Neurology*, vol. 43, no. 11, pp. 2412–2414, Nov. 1993.
- [145] A. J. Saykin *et al.*, “Genetic studies of quantitative MCI and AD phenotypes in ADNI: Progress, opportunities, and plans,” *Alzheimers Dement. J. Alzheimers Assoc.*, vol. 11, no. 7, pp. 792–814, Jul. 2015.
- [146] P. M. Thompson *et al.*, “The ENIGMA consortium: Large-scale collaborative analyses of neuroimaging and genetic data,” *Brain Imag. Behav.*, vol. 8, no. 2, pp. 153–182, Jun. 2014.

- [147] R. J. Bateman *et al.*, “Autosomal-dominant alzheimer’s disease: A review and proposal for the prevention of alzheimer’s disease,” *Alzheimers Res. Therapy*, vol. 3, no. 1, p. 13, Jan. 2011.
- [148] L. A. Farrer *et al.*, “Effects of age, sex, and ethnicity on the association between apolipoprotein e genotype and Alzheimer disease. a meta-analysis. APOE and alzheimer disease meta analysis consortium,” *JAMA*, vol. 278, no. 16, pp. 1349–1356, Oct. 1997.
- [149] K. D. Coon *et al.*, “A high-density whole-genome association study reveals that APOE is the major susceptibility gene for sporadic late-onset alzheimer’s disease,” *J. Clin. Psychiatry*, vol. 68, no. 4, pp. 613–618, 2007.
- [150] M. I. Kamboh *et al.*, “Genome-wide association study of alzheimer’s disease,” *Transl. Psychiatry*, vol. 2, no. 5, May. 2012, Art. no. e117.
- [151] L. Shen and J. Jia, “An overview of genome-wide association studies in alzheimer’s disease,” *Neurosci. Bull.*, vol. 32, no. 2, pp. 183–190, 2016.
- [152] L. Shen *et al.*, “Genetic analysis of quantitative phenotypes in AD and MCI: Imaging, cognition and biomarkers,” *Brain Imag. Behav.*, vol. 8, no. 2, pp. 183–207, Jun. 2014.
- [153] S. Leandrou *et al.*, “Quantitative MRI brain studies in mild cognitive impairment and alzheimer’s disease: A methodological review,” *IEEE Rev. Biomed. Eng.*, vol. 11, pp. 97–111, 2018.
- [154] J. L. Stein *et al.*, “Genome-wide analysis reveals novel genes influencing temporal lobe structure with relevance to neurodegeneration in alzheimer’s disease,” *NeuroImage*, vol. 51, no. 2, pp. 542–554, 2010.
- [155] J. L. Stein *et al.*, “Identification of common variants associated with human hippocampal and intracranial volumes,” *Nat. Genetics*, vol. 44, no. 5, pp. 552–561, May 2012.
- [156] D. P. Hibar *et al.*, “Novel genetic loci associated with hippocampal volume,” *Nat. Commun.*, vol. 8, Jan. 2017, Art. no. 13624.
- [157] N. K. Batmanghelich, A. Dalca, G. Quon, M. Sabuncu, and P. Golland, “Probabilistic modeling of imaging, genetics and diagnosis,” *IEEE Trans. Med. Imag.*, vol. 35, no. 7, pp. 1765–1779, Jul. 2016.
- [158] J. Dukart, F. Sambataro, and A. Bertolino, “Accurate prediction of conversion to alzheimer’s disease using imaging, genetic, and neuropsychological biomarkers,” *J. Alzheimers Dis. JAD*, vol. 49, no. 4, pp. 1143–1159, 2016.
- [159] A. Nazeri *et al.*, “Imaging proteomics for diagnosis, monitoring and prediction of alzheimer’s disease,” *NeuroImage*, vol. 102, no. 2, pp. 657–665, Nov. 2014.
- [160] B. Lehallier *et al.*, “Combined plasma and cerebrospinal fluid signature for the prediction of midterm progression from mild cognitive impairment to alzheimer disease,” *JAMA Neurol.*, vol. 73, no. 2, pp. 203–212, 2016.
- [161] C. R. Jack *et al.*, “Shapes of the trajectories of five major biomarkers of alzheimer’s disease,” *Arch. Neurol.*, vol. 69, no. 7, pp. 856–867, 2012.
- [162] E. Stage *et al.*, “The effect of the top 20 alzheimer disease risk genes on gray-matter density and FDG PET brain metabolism,” *Alzheimers Dement*, vol. 5, pp. 53–66, Dec. 2016.
- [163] E. A. Murphy *et al.*, “CETP polymorphisms associate with brain structure, atrophy rate, and Alzheimer’s disease risk in an APOE-dependent manner,” *Brain Imag. Behav.*, vol. 6, no. 1, pp. 16–26, Mar. 2012.
- [164] E. C. Mormino *et al.*, “Amyloid and APOE  $\varepsilon 4$  interact to influence short-term decline in preclinical alzheimer disease,” *Neurology*, vol. 82, no. 20, pp. 1760–1767, May 2014.
- [165] Y. Y. Lim *et al.*, “Association of  $\beta$ -amyloid and apolipoprotein e  $\varepsilon 4$  with memory decline in preclinical alzheimer disease,” *JAMA Neurol.*, Jan. 2018.
- [166] S. Schreiber *et al.*, “Alzheimer disease signature neurodegeneration and APOE genotype in mild cognitive impairment with suspected non-alzheimer disease pathophysiology,” *JAMA Neurol.*, vol. 74, no. 6, pp. 650–659, Jun. 2017.
- [167] S. Mishra *et al.*, “Longitudinal brain imaging in preclinical alzheimer disease: Impact of APOE  $\varepsilon 4$  genotype,” *Brain J. Neurol.*, vol. 141, no. 6, pp. 1828–1839, Jun. 2018.
- [168] T. Ge, M. Sabuncu, J. Smoller, R. A. Sperling, and E. Mormino, “Dissociable influences of APOE  $\varepsilon 4$  and polygenic risk of AD dementia on amyloid and cognition,” *Neurology*, vol. 90, pp. e1605–e1612, Mar. 2018.
- [169] S. M. Landau *et al.*, “Associations between cognitive, functional, and FDG-PET measures of decline in AD and MCI,” *Neurobiol. Aging*, vol. 32, no. 7, pp. 1207–1218, Jul. 2011.
- [170] D. S. Knopman *et al.*, “ $^{18}\text{F}$ -fluorodeoxyglucose positron emission tomography, aging, and apolipoprotein E genotype in cognitively normal persons,” *Neurobiol. Aging*, vol. 35, no. 9, pp. 2096–2106, Sep. 2014.
- [171] B. S. Langbaum *et al.*, “Categorical and correlational analyses of baseline fluorodeoxyglucose positron emission tomography images from the alzheimer’s disease neuroimaging initiative (ADNI),” *NeuroImage*, vol. 45, no. 4, pp. 1107–1116, May 2009.
- [172] K. Chen *et al.*, “Correlations between FDG PET glucose uptake-MRI gray matter volume scores and apolipoprotein E  $\varepsilon 4$  gene dose in cognitively normal adults: A cross-validation study using voxel-based multimodal partial least squares,” *NeuroImage*, vol. 60, no. 4, pp. 2316–2322, 2012.
- [173] G. T. Stebbins and C. M. Murphy, “Diffusion tensor imaging in alzheimer’s disease and mild cognitive impairment,” *Behav. Neurol.*, vol. 21, no. 1, pp. 39–49, 2009.
- [174] Y. Zhang *et al.*, “Diffusion tensor imaging of cingulum fibers in mild cognitive impairment and Alzheimer disease,” *Neurology*, vol. 68, no. 1, pp. 13–19, Jan. 2007.
- [175] P. Kochunov *et al.*, “Genetic analysis of cortical thickness and fractional anisotropy of water diffusion in the brain,” *Front. Neurosci.*, vol. 5, Oct. 2011, Art. no. 120.
- [176] C. F. Slattery *et al.*, “ApoE influences regional white-matter axonal density loss in alzheimer’s disease,” *Neurobiol. Aging*, vol. 57, pp. 8–17, 2017.
- [177] E. Drucker and K. Kurt, “Pitfalls and limitations in translation from biomarker discovery to clinical utility in predictive and personalised medicine,” *EPMA J.*, vol. 4, no. 1, 2013, Art. no. 7.